Article

Cell

Neural-activity-regulated and glia-mediated control of brain lymphatic development

Graphical abstract

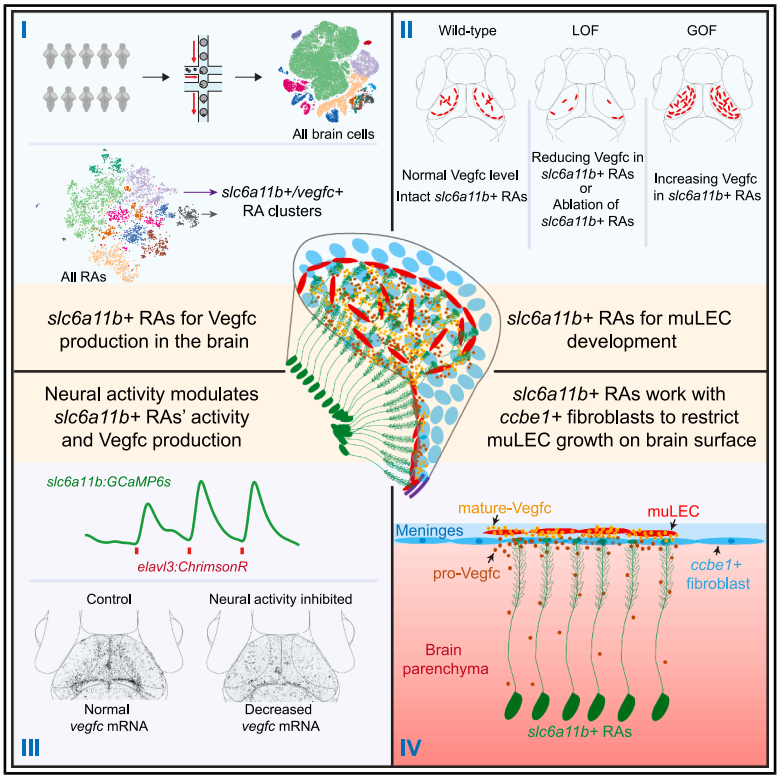

Highlights

- *slc6a11b+* radial astrocytes (RAs) are the primary source of Vegfc in the brain
- Vegfc produced by *slc6a11b+* RAs controls muLEC development
- Neural activity modulates muLEC development via Vegfc expressed in *slc6a11b+* RAs
- *slc6a11b+* RAs work with *ccbe1+* fibroblasts to restrict muLEC growth on brain surface

Authors

Jia Li (李佳), Ming-Jian Liu (刘明剑), Wen-Jie Du (杜文杰), ..., Hua-Xing Zi (訾化星), Han-Bing Shang (尚寒冰), Jiu-Lin Du (杜久林)

Correspondence

lijia@ion.ac.cn (J.L.),
shb11556@rjh.com.cn (H.-B.S.),
forestdu@ion.ac.cn (J.-L.D.)

In brief

Specialized radial astrocytes govern the development of meningeal mural lymphatic endothelial cells that form an immune niche surrounding the zebrafish brain by expressing *vegfc*, which is regulated by neural activity, highlighting critical inter-tissue cellular cooperation in brain lymphatic development.

Li et al., 2025, Cell *188*, 1–17
June 12, 2025
https://doi.org/10.1016/j.cell.2025.04.008

CellPress

Please cite this article in press as: Li et al., Neural-activity-regulated and glia-mediated control of brain lymphatic development, Cell (2025), https://doi.org/10.1016/j.cell.2025.04.008

Cell

CellPress

Article

Neural-activity-regulated and glia-mediated control of brain lymphatic development

Jia Li (李佳),[1,2,8,*] Ming-Jian Liu (刘明剑),[3,7,8] Wen-Jie Du (杜文杰),[4,8] Xiao-Lan Peng (彭小兰),[1] Hao Deng (邓浩),[3] Hua-Xing Zi (訾化星),[1,2] Han-Bing Shang (尚寒冰),[3,5,*] and Jiu-Lin Du (杜久林)[1,2,6,9,*]

[1]Institute of Neuroscience, Key Laboratory of Brain Cognition and Brain-Inspired Intelligence Technology, Center for Excellence in Brain Science and Intelligence Technology, Chinese Academy of Sciences, Shanghai 200031, China
[2]University of Chinese Academy of Sciences, Beijing 100049, China
[3]Department of Neurosurgery, Ruijin Hospital, Shanghai Jiao Tong University School of Medicine, Shanghai 200025, China
[4]Department of Anesthesiology, Huashan Hospital, Fudan University, Shanghai 200040, China
[5]Emergency Medicine Center, Shanghai Institute of Aviation Medicine, Ruijin Hospital, Shanghai Jiao Tong University School of Medicine, Shanghai 200025, China
[6]School of Life Science and Technology, ShanghaiTech University, Shanghai 200031, China
[7]Department of Neurosurgery, Huashan Hospital, Fudan University, Shanghai 200040, China
[8]These authors contributed equally
[9]Lead contact
*Correspondence: lijia@ion.ac.cn (J.L.), shb11556@rjh.com.cn (H.-B.S.), forestdu@ion.ac.cn (J.-L.D.)
https://doi.org/10.1016/j.cell.2025.04.008

SUMMARY

The nervous system regulates peripheral immune responses under physiological and pathological conditions, but the brain's impact on immune system development remains unknown. Meningeal mural lymphatic endothelial cells (muLECs), embedded in the leptomeninges, form an immune niche surrounding the brain that contributes to brain immunosurveillance. Here, we report that the brain controls the development of muLECs via a specialized glial subpopulation, *slc6a11b+* radial astrocytes (RAs), a process modulated by neural activity in zebrafish. *slc6a11b+* RAs, with processes extending to the meninges, govern muLEC formation by expressing vascular endothelial growth factor C (*vegfc*). Moreover, neural activity regulates muLEC development, and this regulation requires Vegfc in *slc6a11b+* RAs. Intriguingly, *slc6a11b+* RAs cooperate with calcium-binding EGF domain 1 (*ccbe1*)+ fibroblasts to restrict muLEC growth on the brain surface via controlling mature Vegfc distribution. Thus, our study uncovers a glia-mediated and neural-activity-regulated control of brain lymphatic development and highlights the importance of inter-tissue cellular cooperation in development.

INTRODUCTION

The nervous and immune systems are two principal systems essential for organismal survival. Increasing evidence indicates that the nervous system can regulate immune responses at both physiological and pathological conditions to help maintain body homeostasis.[1–13] This suggests the presence of anatomical mechanisms that may evolve during development to facilitate this regulation. However, our understanding of the interaction between the nervous and immune systems during development remains limited. In particular, it is unknown whether and how the brain can impact the development of immune systems.

Brain meningeal mural lymphatic endothelial cells (muLECs), initially discovered in zebrafish, are a group of loosely connected LECs residing within the leptomeningeal layer.[14–16] Recently, Prox1+/Lyve1+ LECs in the leptomeninges have also been reported in mice and humans, though more direct evidence is needed to confirm their analog to muLECs.[17,18] Unlike LEC-sealed and -lumenized lymphatic vessels found in the dura mater of vertebrate brains,[19–21] muLECs do not form tubes. Instead, they constitute a single-cell and loosely connected layer meshwork that covers the brain surface.[14–16,22] muLECs are derived from venous endothelial cells (ECs), just like lymphatic vessels in the trunk,[14–16,23] and their development is dependent on the vascular endothelial growth factor C (VEGFC)-VEGF receptor 3 (VEGFR3) signaling pathway.[14–16,19,22] The absorption and drainage of intracisternal injected dyes was found to be through both muLECs and lymphatic vessels but not adjacent blood vessels.[19–21] Furthermore, muLECs in zebrafish can readily endocytose extracellular waste products, including amyloid β, from the brain parenchyma, serving a clearance role in homeostasis and immune functions of the brain.[16,18,22,24]

To address whether the brain can affect the development of muLECs, we took advantage of the optical transparency and genetic manipulation of larval zebrafish, in which the cellular

Please cite this article in press as: Li et al., Neural-activity-regulated and glia-mediated control of brain lymphatic development, Cell (2025), https://doi.org/10.1016/j.cell.2025.04.008

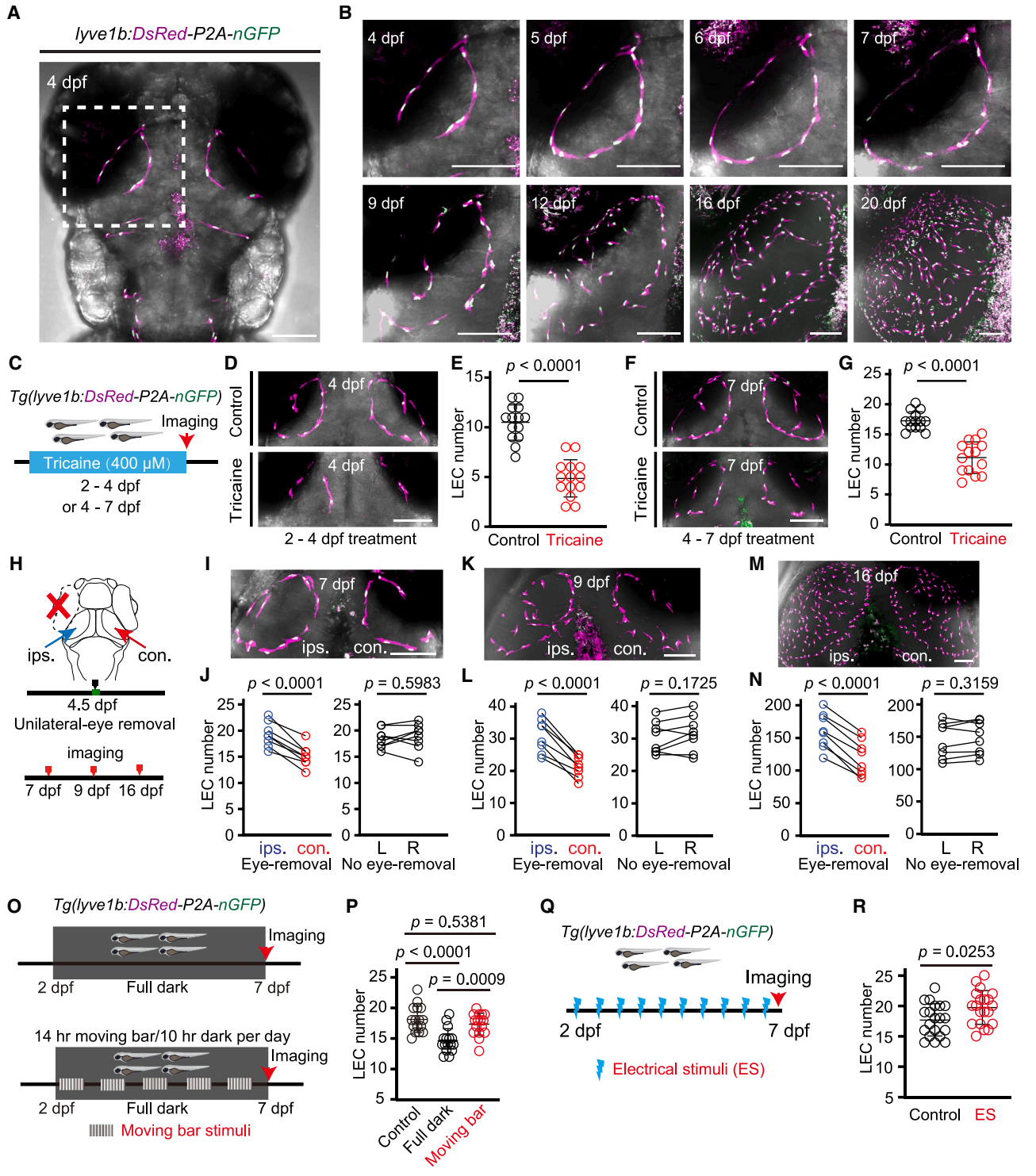

Figure 1. Neural activity regulates muLEC development in zebrafish

(A and B) Developmental dynamics of muLECs in larval zebrafish. *In vivo* time-lapse confocal imaging was performed on a *Tg(lyve1b:DsRed-P2A-nGFP)* larva during 4–20 dpf.

(A) Dorsal view of a projected image merged with bright field at 4 dpf.

(B) muLECs on the left OT shown in the dashed box in (A), at different developmental stages.

(C–G) Effects of tricaine-treatment-based blockade of whole-brain neural activity on muLEC development. Tricaine was bath-applied during 2–4 dpf (D and E) or 4–7 dpf (F and G).

(legend continued on next page)

Please cite this article in press as: Li et al., Neural-activity-regulated and glia-mediated control of brain lymphatic development, Cell (2025), https://doi.org/10.1016/j.cell.2025.04.008

compositions and structural organization of the brain are conserved with mammals,[25–28] and performed *in vivo* time-lapse imaging to explore the regulatory mechanism underlying muLEC development. Through whole-brain single-cell RNA sequencing (scRNA-seq), a subpopulation of glial cells, named as *slc6a11b*+ radial astrocytes (RAs), was identified as the primary source of Vegfc, which is essential for lymphangiogenesis.[29,30] Combining genetic manipulation and *in vivo* imaging, we demonstrated that *slc6a11b*+ RAs and their *vegfc* expression are indispensable for muLEC development. Interestingly, neural activities were found to positively regulate the development of muLECs, and this neural regulation is mediated by *slc6a11b*+ RAs and their *vegfc* expression. To further uncover how *slc6a11b*+ RAs located inside the brain control the development of muLEC distribution outside the brain via Vegfc signaling, we found that calcium-binding EGF domain 1 (*ccbe1*)+ fibroblasts situated on the brain surface cooperate with *slc6a11b*+ RAs to restrict the mature form of Vegfc (mVegfc) on the brain surface. These findings elucidate a control mechanism of brain lymphatic system development via specialized glia and reveal an intriguing role of neural activities in regulating immune system development.

RESULTS

Neural activity regulates zebrafish muLEC development

To investigate the developmental dynamics of muLECs, we generated a transgenic zebrafish line, *Tg(lyve1b:DsRed-P2A-nGFP)* in which the red fluorescent protein dsRed and the nuclear-localized green fluorescent protein (nGFP) are expressed in the cytoplasm and nucleus of LECs, respectively, under the control of the *lyve1b* promoter.[31] We observed that muLECs form a loop at the surface of the boundary between the soma and fiber regions of the optic tectum (OT) in the midbrain from 4 days post-fertilization (dpf) and gradually cover the surface of the OT neuropil (Figures 1A and 1B; see also Bower et al.[14]).

To investigate how the development of muLECs is regulated, we first compared the localizations of muLEC with major types of brain cells, including ECs, fibroblasts, and neurons (Figure S1A). Co-imaging of muLECs and blood vessels in 6-dpf double transgenic *Tg(lyve1b:DsRed);Tg(kdrl:EGFP)* larvae, in which dsRed and enhanced GFP (EGFP) respectively label muLECs and ECs, showed that a significant portion of the muLEC loop did not co-localize with meningeal vessels at this developmental stage (Figure S1B). We then generated a *Ki(pdgfra-GFF);Tg(uas:EGFP)* reporter line to visualize fibroblasts (Figures S1E and S1F), which distributed across the entire brain surface and did not exhibit the distinctive loop-like pattern characteristic of muLECs (Figure S1C). As *pdgfra* is also a marker for oligodendrocyte (OL) precursor cells (OPCs), the reporter line may also label OPCs in the brain.[32] Utilizing the double transgenic *Tg(lyve1b:DsRed);Tg(elavl3:GCaMP6s)* line, in which muLECs and neurons express dsRed and the genetically encoded calcium indicator GCaMP6s, respectively, we observed that the distribution pattern of muLECs mirrors the arrangement of neural fibers terminating on the brain surface (Figure S1D; Video S1). Remarkably, muLECs exhibited a distinctive coverage on the surface of the OT neuropil region (Figures 1B and S1D). The neuropil is composed of the fibers of neurons and glial cells, where neural activity and synaptic transmissions are extensively processed.[25,33] These observations suggest that the central nervous system (CNS) may play a role in regulating muLEC development.

To explore whether the CNS affects muLEC development, we then tested the influences of neural activity. We conducted pharmacological inhibition of neural activity in the entire brain by bath application of the reversible sodium channel blocker tricaine (Figure 1C). Tricaine is known to effectively inhibit action potentials by binding to voltage-gated sodium channels and was used to completely block action potentials in larval zebrafish during development.[34,35] Interestingly, tricaine treatment efficiently suppressed the formation of the muLEC loop and markedly reduced the number of muLECs on the OT surface (Figures 1D–1G; $p < 0.0001$).

As the OT is a hub for visual processing, we then performed unilateral eye removal on larvae to impair neural activities in the contralateral OT (Figures S1G–S1J; $p < 0.05$; see Zhang et al.[33]). Eye removal procedure was operated at 4.5 dpf, and

(C) Experimental design for the tricaine treatment and imaging.
(D–G) Representative images (D and F) and the mean number (E and G) of muLECs on each side of the OT. *In vivo* imaging was performed immediately after tricaine treatment at 4 dpf (D and E) and 7 dpf (F and G). Control group, larvae raised under normal conditions. For each group, muLECs at bilateral OT were examined in 7 larvae in three independent experiments. Each data point indicates the muLEC number in one side of the OT.
(H–N) Effects of unilateral eye removal on muLEC development. Eye removal was performed at 4.5 dpf, and imaging was performed at 7 dpf (I and J), 9 dpf (K and L), or 16 dpf (M and N).
(H) Experimental design for unilateral eye removal and imaging. con., contralateral side; ips., ipsilateral side; red cross, eye removal.
(I, K, and M) Representative images of the eye-removed larvae at 7 (I), 9 (K), and 16 dpf (M).
(J, L, and N) Mean number of muLECs on each side of the OT in the larvae with eye removal (left) and no eye removal (right) at 7 (J), 9 (L), and 16 dpf (N). L, left OT; R, right OT. 8 larvae were examined for each group.
(O and P) Effects of visual experience deprivation and enrichment on muLEC development.
(O) Experimental design for manipulating visual experiences from 2 to 7 dpf and imaging at 7 dpf.
(P) Mean number of muLECs on each side of the OT. Control, 14 h light/10 h dark cycle; full dark, complete darkness; moving bar, 14 h moving bar stimuli/10 h dark cycle. 8 larvae were examined in each group.
(Q and R) Effect of ES on muLEC development.
(Q) Experimental design for ES application from 2 to 7 dpf and imaging at 7 dpf.
(R) Mean number of muLECs on each side of the OT. 10 larvae were examined in each group.
Scale bars: 100 μm in all images. Error bars represent standard deviation (SD). The *p* values were determined using the parametric two-tailed unpaired t test (E, G, and R), the parametric two-tailed paired t test (J, L, and N), and the parametric one-way ANOVA with Tukey's post hoc test (P). Data are represented as mean ± SD. See also Figure S1.

Please cite this article in press as: Li et al., Neural-activity-regulated and glia-mediated control of brain lymphatic development, Cell (2025), https://doi.org/10.1016/j.cell.2025.04.008

muLECs were subsequently imaged at 7, 9, and 16 dpf (Figure 1H). We found a significant decrease in the number of muLECs on the surface of the contralateral OT ($p < 0.0001$), but not the ipsilateral OT, in the eye removal groups compared with the control larvae without eye removal (Figures 1I–1N and S1K). When eye removal was operated at 2.5 dpf, a similar decrease in the muLECs number was observed on the contralateral OT (Figures S1L–S1N; $p < 0.0001$). To moderately reduce visual inputs, we removed the lens of the unilateral eye without destroying the entire eye. Lens removal also resulted in fewer muLECs on the contralateral OT (Figures S1O–S1Q; $p < 0.01$).

We also reduced visual inputs by raising embryos in complete darkness to deprive them of visual experience and observed a significant decrease in the number of muLECs (Figures 1O and 1P; $p < 0.0001$). Conversely, introducing visual stimuli with white moving bars under the dark background led to an increase in the muLECs number (Figures 1O and 1P; $p < 0.001$). We also performed electrical stimulation (ES) on zebrafish larvae to elevate whole-brain neural activities[36] and observed that treated animals exhibited an increase in the number of muLECs (Figures 1Q and 1R; $p < 0.05$). Taken together, these results indicate that neural activities can regulate the development of muLECs.

slc6a11b+ RAs are the major source of Vegfc in the brain

The intriguing regulation of muLEC development by neural activity inspired us to explore its underlying mechanisms. Vegfc and Vegfd are two secreted proteins that play important roles in lymphatic development in vertebrates, including brain lymphatics and trunk LECs.[14,37–40] To identify the candidate cell types with the expression of *vegfc* and *vegfd* in the zebrafish brain, we conducted a comprehensive screening using scRNA-seq data obtained from the entire brain of zebrafish (Figure S2A). In our scRNA-seq study, we performed quality control and obtained transcriptome data from a total of 50,168 single cells at the stages of 6 dpf, 1.5 months post fertilization (mpf), and 3.5 mpf (Figures 2A and S2A). By analyzing the expression of marker genes in combination with cluster analysis, we successfully identified 12 major cell types, including neurons, neural progenitor cells (NPCs), RAs, ECs, mural cells (includes pericytes and smooth muscle cells), LECs, fibroblasts, microglia, OPCs/OLs, erythrocytes, chondrocytes, and ciliated cells (Figures 2A and S2B–S2D). Utilizing the expression of *vegfc* and *vegfd* as indicators, our analysis revealed that RAs are the primary cell type displaying distinctive expressions of *vegfc* and *vegfd* at both developmental and adult stages (Figures 2B, S2E, and S2F).

To corroborate the findings from the scRNA-seq, we generated a knockin line *Ki(vegfc-GFF)* with the method we previously established[41,42] and labeled *vegfc*-expressing cells in zebrafish (Figures S3A and S3B). In alignment with the scRNA-seq data, our imaging results confirmed that the cells expressing *vegfc* in the brain are predominantly RAs (Figure 2C). We observed that *vegfc+* RAs localizing in the midbrain extend their processes to directly target the choroidal vascular plexus (CVP) (Figure S3C), the initial origin site of muLECs.[14–16] Furthermore, to facilitate single-cell visualization of *vegfc+* RAs, we introduced a *uas:CoChR-EGFP-P2A-H2B-mScarlet* plasmid, in which the membrane-localized Chloromonas oogama channelrhodopsin (*CoChR)-EGFP* and the nuclear marker *H2B-mScarlet* are expressed under the control of the *uas* promoter, into one-cell-stage zygotes of *Ki(vegfc-GFF)* (Figure 2D). With this approach, we were able to identify an individual *vegfc+* RA, with its nucleus and processes labeled in red and green, respectively. We observed that the *vegfc+* RAs emanate a primary process, with bushy branches that extended laterally and ventrally toward the CVP or laterally and dorsally to the pial surface of the OT (Figures 2E and S3D; Videos S2 and S3). We also noted *vegfc* expression in fibroblasts, which cover the surface of the brain and lack the looped distribution pattern observed in muLECs (Figures S3E and S3G–S3J). In the trunk, *vegfc* shows expression in the dorsal aorta, the intersegmental arteries, and the horizontal myoseptum (Figure S3F). We then performed multiplexed fluorescent *in situ* RNA hybridization (FISH) using a customized hybridization chain reaction (HCR) method[43] to co-label *vegfc* mRNA with the mRNA of zebrafish *slc1a2b*, an analog of the classical astrocyte marker gene *GLT1* (glial high-affinity glutamate transporter) in mammals,[44] and observed co-localization of *vegfc* mRNA and *slc1a2b* mRNA (Figure S3K), supporting the expression of *vegfc* in the RAs. In addition, we utilized the knockin method to label *vegfd*-expressing cells and observed similar expression patterns in RAs in the brain and fibroblasts on the brain surface (Figures S3L–S3N).

To further elucidate which RA subclusters are the primary cell population expressing *vegfc* and *vegfd*, we conducted a re-clustering analysis of all the RAs (4,476 cells), resulting in 11 subclusters (Figures 2F and S4A–S4D). Notably, the clusters #2 and #7 emerged as the main sources of *vegfc* and *vegfd* expression (Figure 2G). The metascape Gene Ontology (GO) analysis of the two clusters revealed the enriched term of lymphatic vessel development (Figures S4E and S4F). Upon searching for known marker genes of glial cells, we discovered that *slc6a11b*, also known as gamma-aminobutyric acid (GABA) transporter type 3 (GAT3), a gene encoding a sodium-dependent transporter responsible for GABA uptake,[45] was co-expressed with *vegfc* and *vegfd* in both the #2 and #7 clusters (Figure 2G). To specifically label these *slc6a11b+* RAs, we targeted the *slc6a11b* locus and generated a *Ki(slc6a11b-GFF)* knockin line (Figures S4G and S4H). Crossing it with *Tg(uas:EGFP)*, we observed that the *slc6a11b+* cells exhibited identical morphological characteristics to *vegfc+* RAs, displaying the same pattern of processes extending to the surface of the OT neuropil where muLECs are localized (Figure 2H; see also Figure 2C). Unlike *vegfc* expression, *slc6a11b* was found to express only inside of the CNS (including the brain and spinal cord) but not in cells on the brain surface (Figures S4I and S4J; Video S4). To analyze these *slc6a11b+* RAs at a single-cell resolution, we also performed the plasmid injection (Figure 2I). We observed that these RAs exhibited identical morphology to the *vegfc+* RAs, with their process endfeet contacting muLECs (Figures 2J and S4K; see also Figure 2E).

Furthermore, using FISH to simultaneously detect *vegfc* and *slc6a11b* mRNAs in the brain of *Ki(slc6a11b-GFF);Tg(uas:EGFP)* larvae, we observed that *vegfc* mRNA colocalizes with *slc6a11b* mRNA as well as EGFP signals (Figure 2K), indicating that *vegfc* is expressed in *slc6a11b+* RAs in the brain. As *slc6a11b+* RAs are the major source of Vegfc and Vegfd in the

Please cite this article in press as: Li et al., Neural-activity-regulated and glia-mediated control of brain lymphatic development, Cell (2025), https://doi.org/10.1016/j.cell.2025.04.008

CellPress

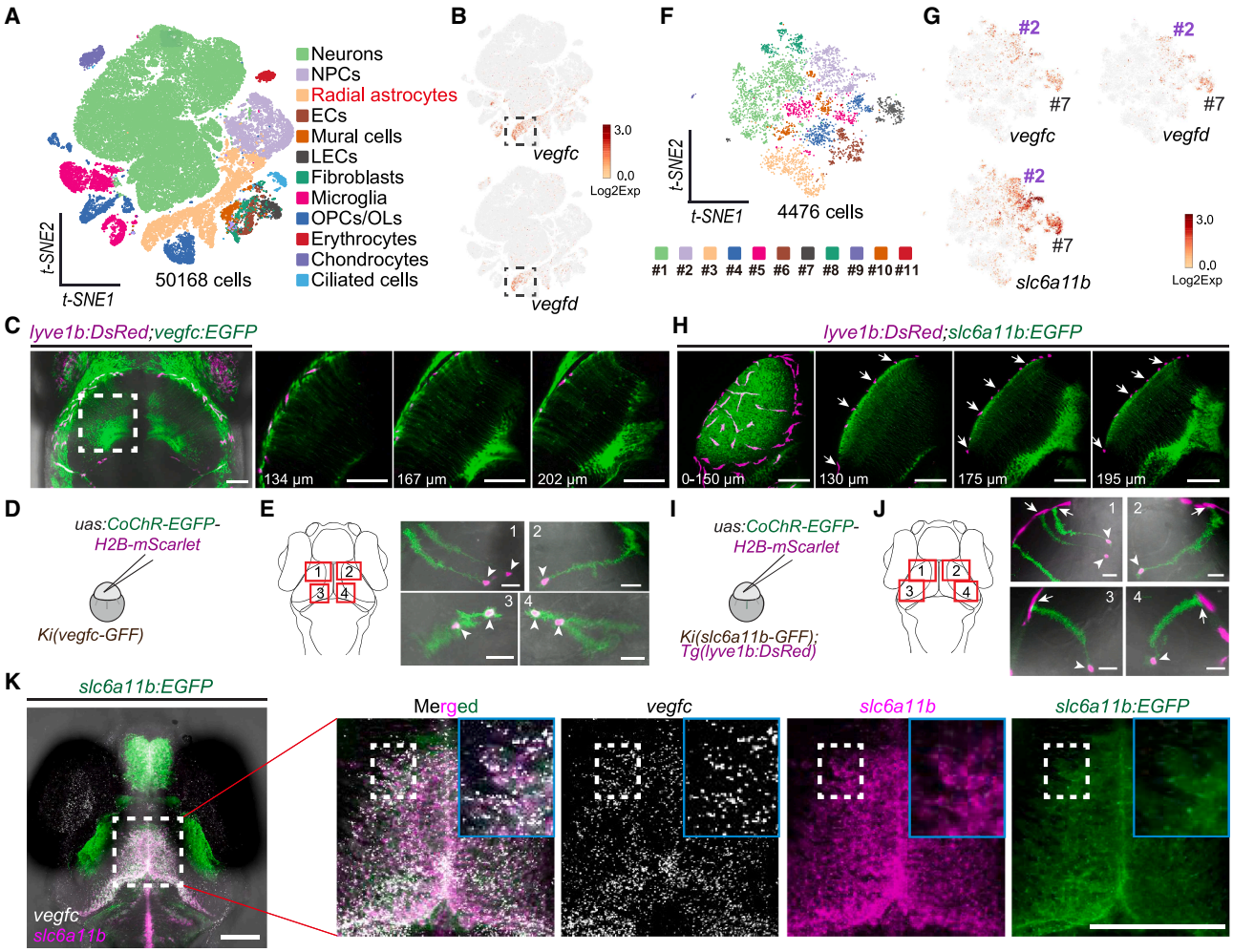

Figure 2. *slc6a11b+* RAs are the major source of Vegfc/Vegfd in the brain

(A) *t*-distributed stochastic neighbor embedding (*t*-SNE) analysis of whole-brain cells of zebrafish at 6 dpf, 1.5 mpf, and 3.5 mpf.

(B) *t*-SNE expression profiles of *vegfc* and *vegfd* in whole-brain cells.

(C) Dorsal view of *vegfc+* RAs in a *Tg(lyve1b:DsRed);Ki(vegfc-GFF);Tg(uas:EGFP)* (abbreviated as *lyve1b:DsRed;vegfc:EGFP*) larva at 10 dpf. The left image is a projected z stacked dorsal-view image showing inside of the brain. The right three images, taken from the dashed box in the left image, are slide images at depths of 134, 167, and 202 μm from the dorsal skin, showing RAs at these respective depths.

(D and E) Sparse labeling and *in vivo* imaging of individual *vegfc+* RAs for visualizing their distinct morphology and localization.

(D) Cartoon depicting the injection of the plasmid *uas:CoChR-EGFP-P2A-H2B-mScarlet* into a fertilized egg of *Ki(vegfc-GFF)* for sparse labeling of individual *vegfc+* RAs.

(E) Left: cartoon depicting the imaging locations (the four red boxes). Right: images of individual *vegfc+* RAs from the four positions marked in the left, showing their distinct morphology.

(F) *t*-SNE analysis of RAs.

(G) *t*-SNE expression profiles of *vegfc*, *vegfd*, and *slc6a11b* in RAs, showing the co-expression of these three genes in the #2 and #7 subclusters.

(H) Dorsal view of muLECs (red) and *slc6a11b+* RAs (green) in the left OT. *In vivo* confocal imaging was performed on a *Tg(lyve1b:DsRed);Ki(slc6a11b-GFF);Tg(uas:EGFP)* (abbreviated as *lyve1b:DsRed;slc6a11b:EGFP*) larva at 10 dpf to label muLECs and *slc6a11b+* RAs. The left image (0–150 μm) is a projected z stacked dorsal-view image with a thickness of 150 μm, spanning from the dorsal skin to the ventral side of the brain. The right three images, taken at depths of 130, 175, and 195 μm from the dorsal skin, show slide images at the respective depths. The white arrows indicate muLECs at the brain surface.

(I and J) Sparse labeling and *in vivo* imaging of individual *slc6a11b+* RAs for visualizing their distinct morphology and localization.

(I) Cartoon depicting the sparse labeling of individual *slc6a11b+* RAs.

(J) Left: cartoon depicting the imaging locations (the four red boxes). Right: images of individual *slc6a11b+* RAs at the four locations, showing that the endfeet of RAs contact with muLECs at the surface of the OT (indicated by white arrows). White arrowheads mark the nucleus of *slc6a11b+* RAs.

(K) z stacked image showing the co-labeling of *vegfc* and *slc6a11b* mRNAs in *slc6a11b+* RAs. Multiplexed FISH was performed on a whole-mount 6-dpf *slc6a11b:EGFP* larva by using a customized HCR method with designed probes of *vegfc* (white) and *slc6a11b* (magenta). The left panel shows co-localization of *vegfc* and *slc6a11b* mRNAs in RAs. The four right panels represent images of the boxed region in the left. Magnified views of the dashed-boxed areas within these panels are displayed in the upper-right corner, highlighting the spatial overlap of *vegfc* and *slc6a11b* transcripts in RAs.

Scale bars: 20 μm (E and J) and 100 μm (C, H, and K).

See also Figures S2, S3, and S4.

Please cite this article in press as: Li et al., Neural-activity-regulated and glia-mediated control of brain lymphatic development, Cell (2025), https://doi.org/10.1016/j.cell.2025.04.008

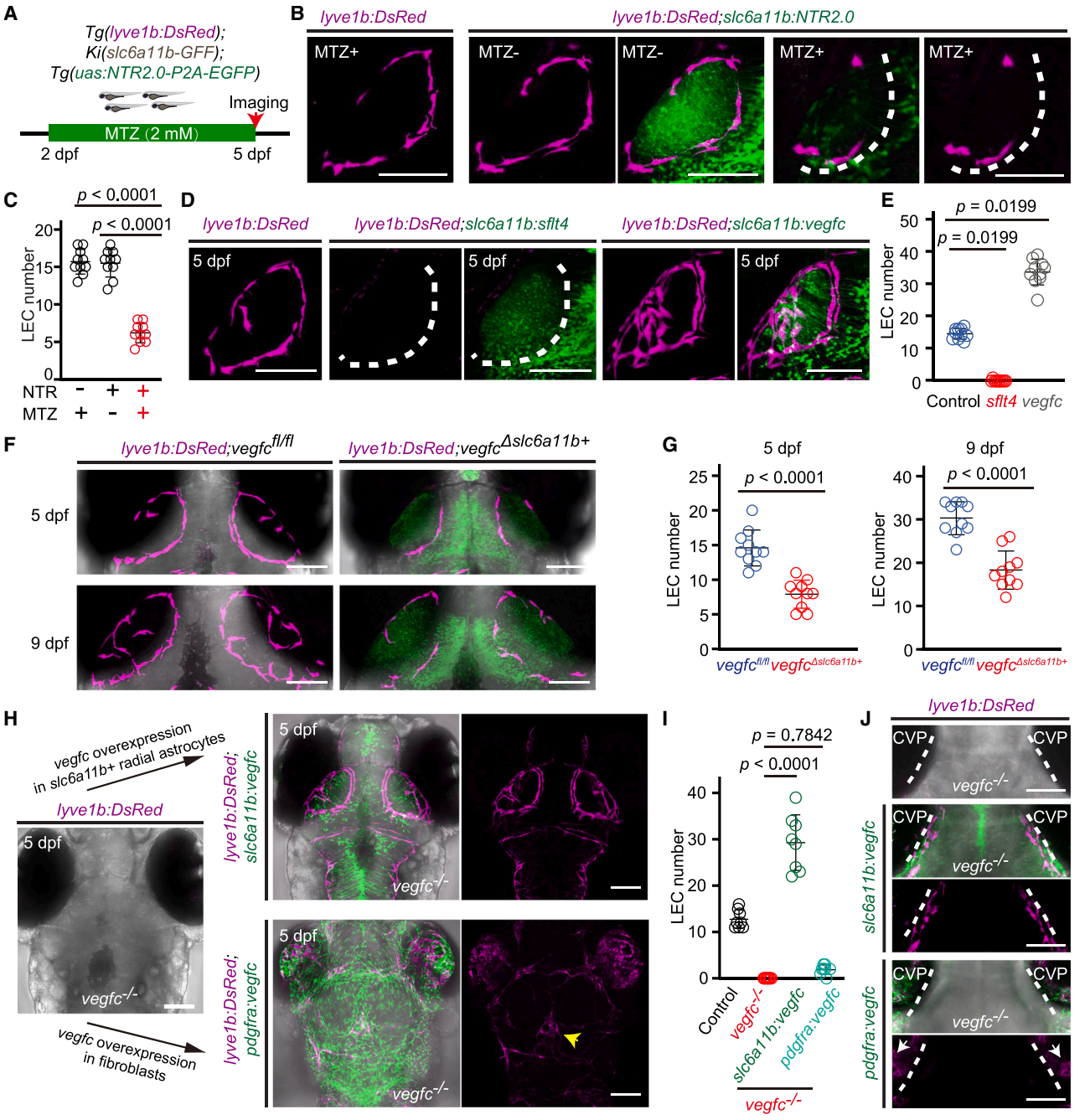

Figure 3. *Vegfc* expressed by *slc6a11b+* RAs is essential for muLEC development

(A–C) Effects of the *slc6a11b+* RAs ablation on muLEC development. MTZ was bath-applied during 2–5 dpf to ablate *slc6a11b+* RAs in *Tg(lyve1b:DsRed);Ki(slc6a11b-GFF);Tg(uas:NTR2.0-P2A-EGFP)* (abbreviated as *lyve1b:DsRed;slc6a11b:NTR2.0*) larvae.

(A) Experimental design for MTZ treatment and imaging.

(B and C) Representative images (B) and the mean number (C) of muLECs on one side of OT. Each data point indicates the muLEC number in one side of the OT.

(D and E) Effects of the *slc6a11b+* RA-specific manipulations of Vegfc-Vegfr3 signaling on muLEC development. Representative images (D) and the mean number (E) of muLECs on one side of the OT.

(F and G) Effects of conditional knockout of *vegfc* in *slc6a11b+* RAs on muLEC development. Representative images of bilateral muLEC loops (F) and the mean number of muLECs on each side of the OT (G) in the control *lyve1b:DsRed;vegfc*$^{fl/fl}$ larvae and the *lyve1b:DsRed;vegfc*$^{\Delta slc6a11b+}$ larvae at 5 and 9 dpf.

(H–J) Rescue effects on the loss-of-muLEC phenotype in *vegfc*$^{-/-}$ by overexpression of *vegfc* in *slc6a11b+* RAs or fibroblasts. *Ki(slc6a11b-GFF);Tg(uas:mNeonGreen-P2A-vegfc)* (abbreviated as *slc6a11b:vegfc*) was used for *vegfc* overexpression in *slc6a11b+* RAs, and *Ki(pdgfra-GFF);Tg(uas:mNeonGreen-P2A-vegfc)* (abbreviated as *pdgfra:vegfc*) was used for *vegfc* overexpression in fibroblasts. Images were taken at 5 dpf.

(legend continued on next page)

Please cite this article in press as: Li et al., Neural-activity-regulated and glia-mediated control of brain lymphatic development, Cell (2025), https://doi.org/10.1016/j.cell.2025.04.008

brain, *slc6a11b* can serve as a specific marker for labeling *vegfc*- and *vegfd*-expressing RAs in the brain. Henceforth, we refer to the *vegfc+/vegfd+* RAs as *slc6a11b+* RAs.

slc6a11b+ RAs are essential for muLEC development via the Vegfc-Vegfr3 signaling pathway

To gain insights into whether the *slc6a11b+* RAs regulate muLEC development, we first performed loss-of-function experiments with ablation of the *slc6a11b+* RAs using the nitroreductase (NTR)/metronidazole (MTZ) system (Figure 3A).[46] We generated a line of *Tg(uas:NTR2.0-P2A-EGFP)* on the *Tg(slc6a11b-GFF)* background and crossed it to *Tg(lyve1b:DsRed)*, getting the progeny embryos of *Tg(lyve1b:DsRed);Tg(slc6a11b-GFF);Tg(uas:NTR2.0-P2A-EGFP)* in which NTR2.0 is expressed in *slc6a11b+* RAs. After MTZ treatment from 2 to 5 dpf, *slc6a11b+* RAs were efficiently ablated (comparing the third and fifth images on top in Figure 3B), and muLEC development was markedly suppressed, as evidenced by the failure of the muLEC loop to form and a significant decrease in muLEC numbers (Figures 3B and 3C; $p < 0.0001$).

As the Vegfc-Vegfr3 signaling pathway is essential for lymphatics development,[14,16] we then manipulated this signaling pathway specifically in the *slc6a11b+* RAs (Figure 3D). We first blocked the Vegfc-Vegfr3 pathway by using the soluble version *sflt4* of the Flt4/Vegfr3 receptor as a ligand trap.[30] The ectopic expression of *sflt4* in *slc6a11b+* RAs completely blocked the development of muLECs (Figures 3D and 3E; $p < 0.05$). By contrast, we found that *vegfc* overexpression in *slc6a11b+* RAs significantly enhanced the development of muLECs, including the earlier formation of the muLEC loop and the increased number of muLECs (Figures 3D and 3E; $p < 0.05$). These results together indicate that the *slc6a11b+* RAs are essential for muLEC development via the Vegfc-Vegfr3 signaling pathway.

vegfc in *slc6a11b+* RAs is essential for muLEC development

To further demonstrate the cell-type-specific role of *vegfc* for muLEC development, we carried out conditional knockout of *vegfc* in *slc6a11b+* cells. Previous studies showed that Vegfc and Vegfd work redundantly for muLEC development by characterizing zebrafish carrying the *vegfc* point-mutation allele[47] or *vegfd* deletion allele,[37] because homozygous mutants of the each gene failed to completely suppress muLEC development.[14]

Using CRISPR-Cas9, we first generated a *vegfc* deletion allele ($vegfc^{-/-}$) and a *vegfd* deletion allele ($vegfd^{-/-}$), both of which caused reading frameshifts (Figures S5A and S5B). We found that the brain lymphatics, including muLECs and intracranial lymphatic vessels, were completely lost in the homozygous $vegfc^{-/-}$ mutant but not in the homozygous $vegfd^{-/-}$ mutant (Figures S5C and S5D). The different phenotypes of muLECs between the *vegfc* point-mutation allele $vegfc^{hu5055}$ and our *vegfc* deletion knockout are probably because the point-mutation is not a full loss-of-function allele.[47] Our results indicate that Vegfc, but not Vegfd, is required for muLEC development,[16] consistent with the findings in mice showing that loss of Vegfc, but not Vegfd, impairs meningeal lymphatic vessel development.[38]

Next, we generated a floxed allele $vegfc^{fl}$ to achieve conditional knockout of *vegfc* in *slc6a11b+* RAs by using the method we recently developed (Figures S5E and S5F).[48] To evaluate $vegfc^{fl}$ functionality, we crossed $vegfc^{+/fl}$ to the above $vegfc^{+/-}$ adults. The trans-heterozygous $vegfc^{fl/-}$ larvae exhibited normal muLEC development and appeared indistinguishable from the $vegfc^{+/-}$ siblings (Figures S5G and S5H). Consistently, $vegfc^{fl/fl}$ larvae also showed normal muLEC development (Figures S5G and S5H), and the $vegfc^{fl/fl}$ adults were viable and fertile. By contrast, the larvae of $vegfc^{fl/fl}$ injected with a zebrafish codon-optimized *Cre* mRNA (*zCre*) at one-cell stage showed the absence of muLECs, whereas the wild-type siblings were normal with *zCre* mRNA injection (Figures S5I and S5J). These results show that $vegfc^{fl}$ does not interrupt the normal function of Vegfc and the Cre-dependent deletion of the exon 4 to exon 7 in $vegfc^{fl/fl}$ phenocopies $vegfc^{-/-}$ knockout mutants. Thus, $vegfc^{fl}$ can be used as a conditional loss-of-function deletion allele following Cre-mediated deletion.

To achieve Cre-mediated conditional knockout, we made a line of *Tg(uas:mNeonGreen-P2A-Cre)* (referred to as *Tg(uas:Cre)*) for the specific expression of *Cre* in the *slc6a11b* RAs by crossing to the *Ki(slc6a11b-GFF)* line. We proved that Cre expression within *slc6a11b+* RAs cells did not exert obvious influence on muLEC development (see Figures S5G, right, and S5H). To test the Cre recombinase efficiency in the glia, we crossed the *Ki(slc6a11b-GFF);Tg(uas:Cre)* (referred to as *Ki(slc6a11b:Cre)*) to *Tg(actb2:loxP-BFP-polyA-loxp-DsRed)* (referred to as *Tg(actb2:BSR)*) in which the fluorescent protein expression is switched from the blue fluorescent protein (BFP) to dsRed after Cre-mediated recombination (Figure S6A).[49] A substantial number of switched dsRed+ glia were observed (Figure S6B), demonstrating the effective functionality of the Cre-LoxP-based recombinase system within the *slc6a11b+* RAs.

By making use of *Ki(slc6a11b:Cre)* with $vegfc^{fl/fl}$ background, we observed that the deletion of *vegfc* within *slc6a11b+* RAs ($vegfc^{\Delta slc6a11b+}$) led to a substantial suppression of muLEC

(H and I) Representative images (H) and the mean number (I) of the rescue effects. Left (H): dorsal view of a projected image merged with bright field in a $vegfc^{-/-}$ larva. Upper right (H): representative images of a *slc6a11b:vegfc* larva with $vegfc^{-/-}$ background. Lower right (H): representative images of bilateral OT in a *pdgfra:vegfc* larva with $vegfc^{-/-}$ background. The yellow arrowhead in (H) indicates ectopic LECs on the brain surface.

(J) Rescue effects on the loss-of-muLEC around CVP. Representative images of the bilateral CVP in a $vegfc^{-/-}$ larva (upper image), *slc6a11b:vegfc* larva with $vegfc^{-/-}$ background (two images at center), and *pdgfra:vegfc* larva with $vegfc^{-/-}$ background (bottommost two images). The white arrowheads mark non-specific fluorescence on the eyes.

Scale bars: 100 μm in all images. Error bars represent SD. The *p* values were determined using the parametric one-tailed one-way ANOVA with Tukey's post hoc test (C), non-parametric one-tailed Kruskal-Wallis test with post hoc Dunnett's test (E and I), and parametric two-tailed paired t test (G). Data are represented as mean ± SD.

See also Figures S5 and S6.

Please cite this article in press as: Li et al., Neural-activity-regulated and glia-mediated control of brain lymphatic development, Cell (2025), https://doi.org/10.1016/j.cell.2025.04.008

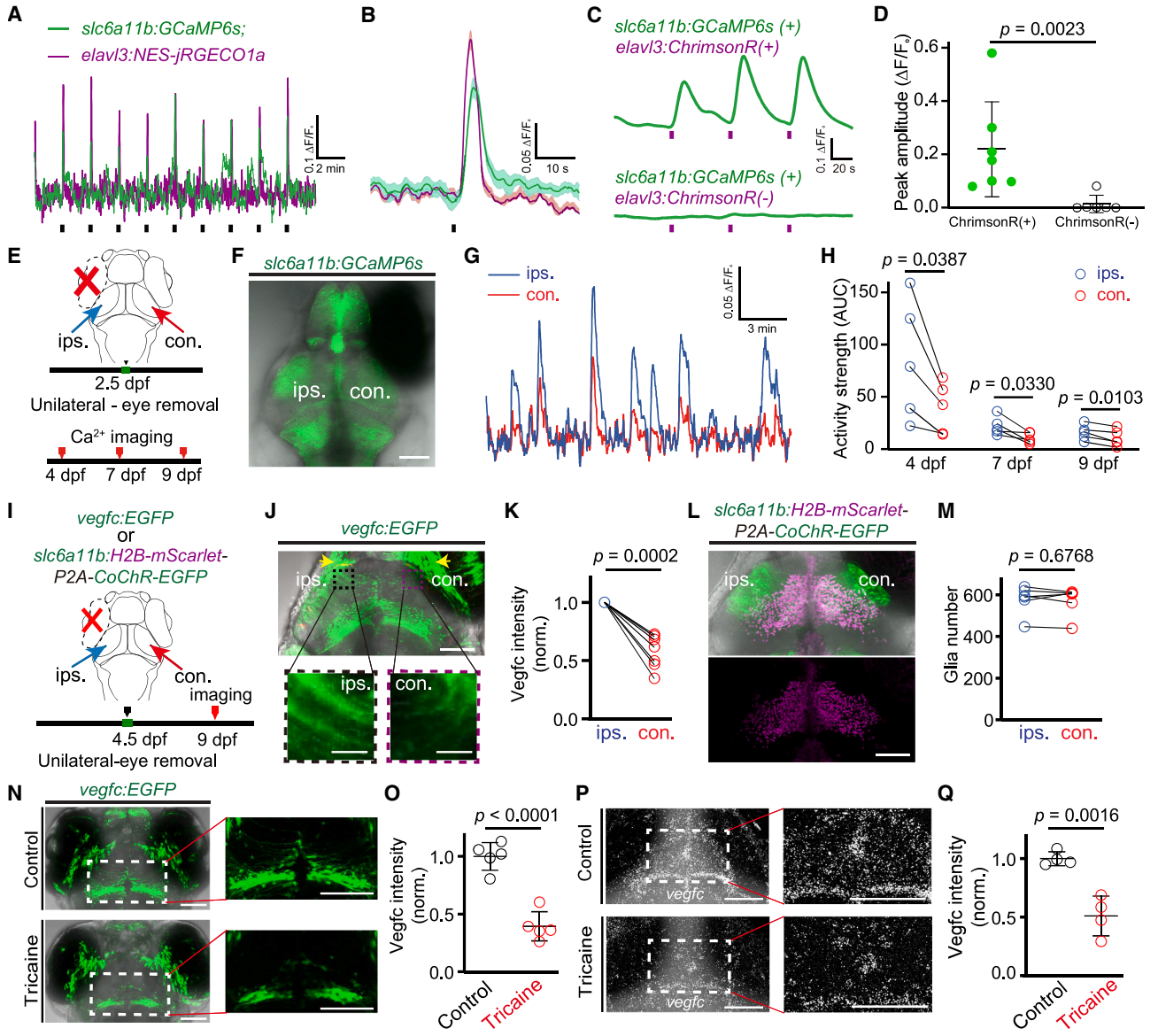

Figure 4. Activity and *vegfc* expression of *slc6a11b+* RAs are coupled to neural activity

(A and B) Ca^{2+} activities of both *slc6a11b+* RAs and neurons in the OT. Simultaneous dual-color Ca^{2+} imaging was performed on *Ki(slc6a11b-GFF);Tg(uas:GCaMP6s);Tg(elavl3:NES-jRGECO1a)* zebrafish larvae at 7 dpf, which express the green fluorescent Ca^{2+} indicator GCaMP6s in *slc6a11b+* RAs and the red fluorescent Ca^{2+} indicator jRGECO1a in neurons, respectively.

(A) Representative Ca^{2+} activities of *slc6a11b+* RAs (green) and neurons (red) in the OT in response to repetitive flash stimuli (black short bars) in a 7 dpf larva. The experiment was performed in 5 larvae fish, all of which exhibited the same pattern of Ca^{2+} activities in RAs and neurons.

(B) Mean traces of flash-evoked Ca^{2+} activities shown in (A). The solid lines indicate the averaged responses and the shaded areas indicate the standard error.

(C and D) Ca^{2+} activities of *slc6a11b+* RAs evoked by optogenetic activation of neurons. Bilateral eyes were removed to avoid optogenetic laser-evoked responses in neurons and glia.

(C) Ca^{2+} activities of *slc6a11b+* RAs evoked by three consecutive optogenetic stimulations (red short bars) in larvae with or without ChrimsonR expression.

(D) Summary of the peak amplitude of evoked Ca^{2+} activities in *slc6a11b+* RAs.

(E–H) Effects of unilateral eye removal on the activities of *slc6a11b+* RAs in the contralateral OT.

(E) Experimental design for unilateral eye removal and Ca^{2+} imaging of *slc6a11b+* RAs.

(F) Dorsal view of the brain in a 7-dpf *slc6a11b:GCaMP6s* larva with left eye removal.

(G) Spontaneous Ca^{2+} activities of *slc6a11b+* RAs on the ipsilateral (blue) and contralateral (red) side of the OT.

(H) Summary of data showing the activity strength (area under curve [AUC]) of spontaneous Ca^{2+} activities in *slc6a11b+* RAs in contralateral and ipsilateral OT.

(I–M) Effects of unilateral eye removal on *vegfc* expression in *slc6a11b+* RAs.

(I) Experimental design for unilateral eye removal and imaging.

(legend continued on next page)

Please cite this article in press as: Li et al., Neural-activity-regulated and glia-mediated control of brain lymphatic development, Cell (2025), https://doi.org/10.1016/j.cell.2025.04.008

development on the OT surface (Figures 3F and 3G; $p < 0.0001$). In addition, the number of LECs near the CVP also decreased (Figures S6C and S6D; $p < 0.0001$). As the CVP is the origin site where muLECs differentiate and then migrate dorsally to form the muLEC loop on the OT neuropil, these results indicate that *vegfc* in *slc6a11b+* RAs is crucial for muLEC development on the surface of the OT neuropil in the meninges, possibly via regulating the processes of its differentiation, migration, and/or loop formation. As *vegfc* is expressed in *slc6a11b+* RAs as well as fibroblasts covering the brain surface (see Figures S3I and S3J), we further investigated whether the expression of *vegfc* in these RAs and the fibroblasts could rescue the muLEC absence phenotype in *vegfc*$^{-/-}$ larvae. We found that specific overexpression of *vegfc* in *slc6a11b+* Ras, but not fibroblasts, successfully restored both the muLEC loop formation on the OT surface (Figures 3H and 3I) and their appearance near the CVP (Figure 3J) in *vegfc*$^{-/-}$ larvae. In addition, we performed conditional knockout of *vegfc* specifically in *pdgfra+* fibroblasts and observed a modest reduction in the number of muLECs (Figures S6E and S6F), although to a lesser extent compared with conditional knockout of *vegfc* in *slc6a11b+* RAs (see Figures 3F and 3G).

Taken together, these results suggest that *slc6a11b+* RAs play a major role in determining muLEC development, and *pdgfra+* fibroblasts play a secondary role in this process. Given that the fiber terminals of *slc6a11b+* RAs are positioned in close proximity to *pdgfra+* fibroblasts on the brain surface (see Video S2), it is of interest in the future to explore how these RAs and fibroblasts coordinate Vegfc production for muLEC development in the meninges.

Activity and Vegfc expression of *slc6a11b+* RAs are coupled to neural activity

To examine whether *slc6a11b+* RAs and their *vegfc* are involved in the regulation of muLEC development by neural activity, we performed simultaneous dual-color Ca^{2+} imaging on *Ki(slc6a11b-GFF);Tg(uas:GCaMP6s);Tg(elavl3:NES-jRGECO1a)* zebrafish larvae, which express the green fluorescent Ca^{2+} indicator GCaMP6s in *slc6a11b+* RAs and the red fluorescent Ca^{2+} indicator jRGECO1a in neurons, respectively. Similar to neuronal fibers in the OT neuropil, *slc6a11b+* RAs responded to light stimuli with increased Ca^{2+} activities (Figures 4A and 4B). To delve deeper into the relationship between neurons and *slc6a11b+* RAs, we optogenetically activated neurons in the OT and simultaneously performed Ca^{2+} imaging of *slc6a11b+* RAs in *Ki(slc6a11b-GFF);Tg(uas:GCaMP6s);Tg(elavl3:ChrimsonR-tdTomato)* larvae in which *slc6a11b+* RAs and neurons express GCaMP6s and the channelrhodopsin ChrimsonR fused with the red fluorescent protein tdTomato, respectively (Figure 4C). We observed that neuronal activation induced by optogenetics led to a corresponding increase in Ca^{2+} activities in *slc6a11b+* RAs (Figures 4C and 4D).

Given the significant suppression of muLEC development observed on the contralateral side of the brain following unilateral eye removal (see Figures 1H–1N and S1L–S1N), we sought to investigate whether the activities of the *slc6a11b+* RAs are also influenced by the interruption of visual experience. We performed unilateral eye removal at 2.5 dpf and subsequently imaged spontaneous Ca^{2+} activities in *slc6a11b+* RAs at 4, 7, and 9 dpf (Figures 4E and 4F). As observed in OT neurons (see Figures S1G–S1I), spontaneous Ca^{2+} activities of *slc6a11b+* RAs in the contralateral OT were impaired in comparison with those in the ipsilateral OT (Figures 4G and 4H; $p < 0.05$). These findings collectively indicate that the activity of *slc6a11b+* RAs is coupled to neural activities in the brain.

We then investigated whether neural activity influences *vegfc* expression in *slc6a11b+* RAs. We examined the effects of neural activity reduction on *vegfc* expression in the brain. The *Ki(vegfc-GFF);Tg(uas:EGFP)* (referred to as *Ki(vegfc:EGFP)*) was used to indicate the level of *vegfc* expression. Unilateral eye removal experiments revealed a significant decrease of the *vegfc* expression in RAs' fibers at the contralateral side (Figures 4I–4K; $p < 0.001$), whereas the number of *slc6a11b+* RAs remained unchanged (Figures 4L and 4M). Furthermore, we employed the *Ki(vegfc:EGFP)* reporter line and FISH to quantify *vegfc* expression in the larvae following tricaine treatment. The results showed a significant decrease in both *vegfc:EGFP* fluorescence and *vegfc* mRNA levels upon neural activity blockade (Figures 4N–4Q). Together, these findings indicate that reduced neural activity leads to decreased *vegfc* expression in *slc6a11b+* RAs.

(J and K) Representative images (J) and the normalized *vegfc* expression of *vegfc+* RAs (K) in the OT of a 9-dpf *vegfc:EGFP* larva with left eye removal. The bottom-left two images in (J) are enlarged view of the areas indicated by the dashed boxes in the upper-left image, with the black box indicating the ipsilateral side and the red box indicating the contralateral side. The yellow arrows indicate the fluorescence signals in fibroblasts on the brain surface. The mean fluorescent intensity (FI) of *vegfc+* fibers from three areas (48 × 48 μm) on each side of the OT was analyzed using ImageJ. The fold change was calculated as (cont. FI − background FI)/(ips. FI − background FI), with the ipsilateral side normalized to 1.

(L and M) Representative images (L) and the number (M) of *slc6a11b+* RAs in the OT of a 9-dpf *slc6a11b:H2B-mScarlet-P2A-CoChR-EGFP* larva with left eye removal. The number of *slc6a11b+* RAs was counted by using ImageJ based on the nuclear-localized red H2B-mScarlet signal.

(N–Q) Effects of tricaine treatment on *vegfc* expression in the brain.

(N and O) Representative images (N) and the normalized *vegfc* expression of *vegfc+* RAs (O) in the OT of 4-dpf *vegfc:EGFP* larvae under control or tricaine treatment from 2 to 4 dpf, as shown in Figure 1C. In (O), the mean FI of *vegfc:EGFP* signals from one area (the dashed box in N, 294 × 159 μm) in the OT was analyzed using ImageJ. The normalized fold change was calculated as (FI − background FI)/(average of the control FI − background FI).

(P and Q) Representative images (P) and the normalized *vegfc* mRNA expression (Q) detected by FISH in the OT of 4-dpf wild-type (WT) larvae under control or tricaine treatment from 2 to 4 dpf. In (Q), the mean FI of *vegfc* mRNA by FISH from one area (the dashed box in P, 193 × 124 μm) in the OT was analyzed using ImageJ. The normalized fold change was calculated as (FI − background FI)/(average of the control FI − background FI).

Scale bars: 20 μm (J, bottom images), 100 μm (F, J [upper image], L, N, and P). Error bars represent SD. The *p* values were determined using the two-tailed non-parametric Mann-Whitney U test (D), the parametric two-tailed paired t test (H, K, and M), and the parametric two-tailed unpaired t test (O and Q), data are represented as mean ± SD.

Please cite this article in press as: Li et al., Neural-activity-regulated and glia-mediated control of brain lymphatic development, Cell (2025), https://doi.org/10.1016/j.cell.2025.04.008

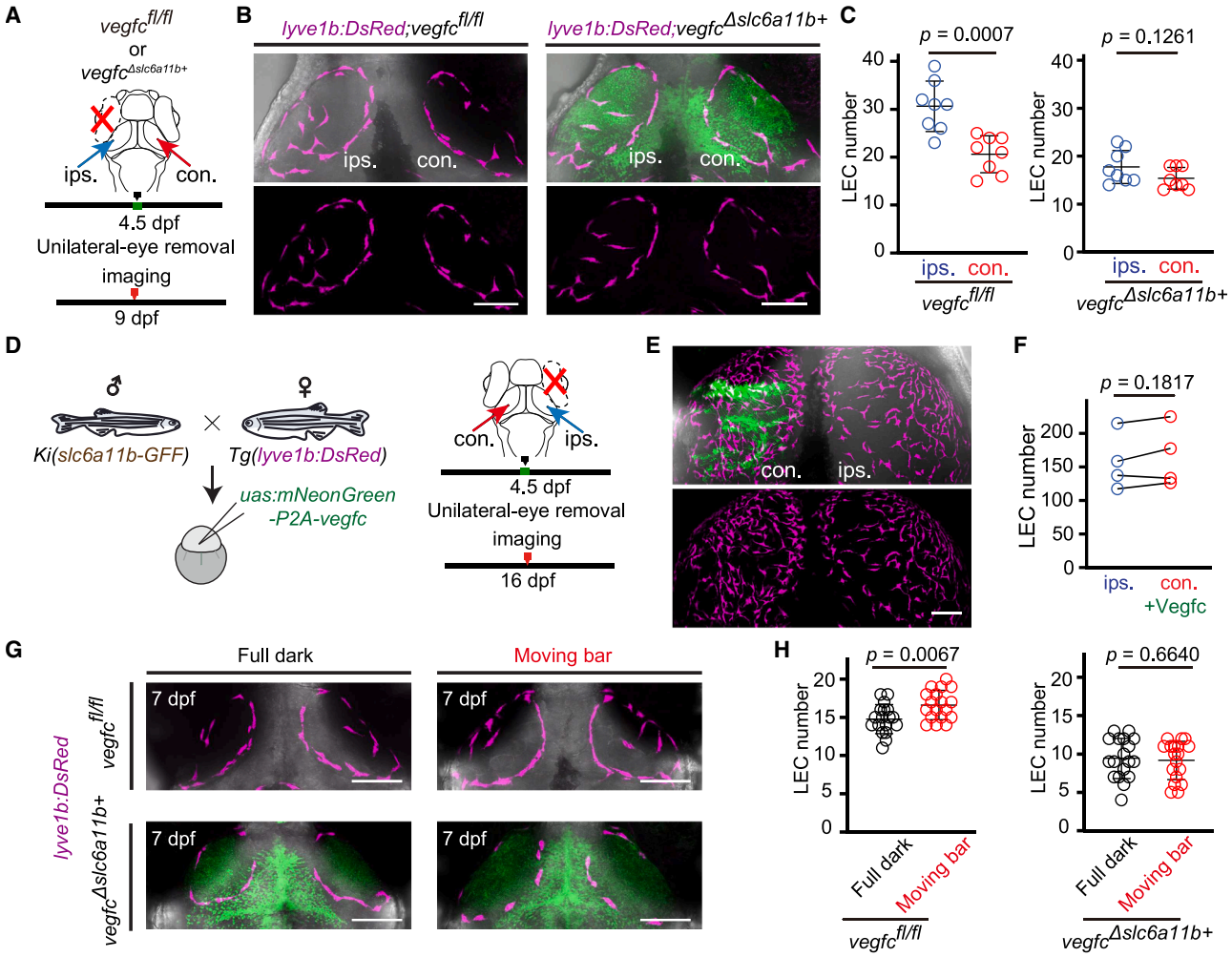

Figure 5. Neural activity regulates muLEC development through *vegfc* expressed in *slc6a11b+* RAs

(A–C) Conditional knockout of *vegfc* in *slc6a11b+* RAs occludes the eye-removal-induced impairment of muLEC development.

(A) Experimental design for unilateral eye removal on $vegfc^{fl/fl}$ and $vegfc^{\Delta slc6a11b+}$ larvae.

(B and C) Representative images of bilateral muLEC loops (B) and the mean number of muLECs (C) on each side of the OT in 9-dpf $vegfc^{fl/fl}$ and $vegfc^{\Delta slc6a11b+}$ larvae with unilateral eye removal.

(D–F) Mosaic overexpression of *vegfc* in *slc6a11b+* RAs rescues the eye-removal-induced impairment of muLEC development.

(D) Cartoon depicting the injection of the *uas:mNeonGreen-P2A-vegfc* plasmid into the fertilized egg of *Tg(lyve1b:DsRed);Tg(slc6a11b-GFF)* for mosaically overexpressing *vegfc* in *slc6a11b+* RAs. Right: experimental design. Larvae with unilateral overexpression of *vegfc* in the OT were used for eye removal at the contralateral side.

(E and F) Representative images (E) and the mean number of muLECs (F) on each side of the OT in a 16-dpf larvae. ips, ipsilateral side without *vegfc* expression; con. + Vegfc, contralateral side with mosaic overexpression of *vegfc*.

(G and H) Conditional knockout of *vegfc* in *slc6a11b+* RAs occludes the moving-bar-induced enhancement of muLEC development. Representative images of bilateral muLEC loops (G) and the mean number of muLECs (H) on each side of the OT in 7-dpf $vegfc^{fl/fl}$ and $vegfc^{\Delta slc6a11b+}$ larvae raised in full dark without or with moving bar stimulation.

Scale bars: 100 μm in all images. Error bars represent SD. The *p* values were determined using the parametric two-tailed unpaired t test (C and H, left), the parametric two-tailed paired t test (F), and the two-tailed non-parametric Mann-Whitney U test (H, right). Data are represented as mean ± SD.

muLEC development regulation by neural activity is mediated by *vegfc* in *slc6a11b+* RAs

Next, we examined whether neural activity regulates muLEC development via *vegfc* in the *slc6a11b+* RAs. We therefore conducted unilateral eye removal experiments on larvae with *vegfc* conditional knockout in *slc6a11b+* RAs ($vegfc^{\Delta slc6a11b+}$) (Figure 5A). We found that reducing neural activity by eye removal could not further decrease the number of muLECs in $vegfc^{\Delta slc6a11b+}$ in comparison with $vegfc^{fl/fl}$ (Figures 5B and 5C). Notably, mosaic overexpression of *vegfc* in *slc6a11b+* RAs on the contralateral OT was able to rescue the decrease in muLEC numbers caused by eye removal (Figures 5D–5F). Furthermore, elevating neural activity by moving bars could no longer increase the number of muLECs in $vegfc^{\Delta slc6a11b+}$ larvae

Please cite this article in press as: Li et al., Neural-activity-regulated and glia-mediated control of brain lymphatic development, Cell (2025), https://doi.org/10.1016/j.cell.2025.04.008

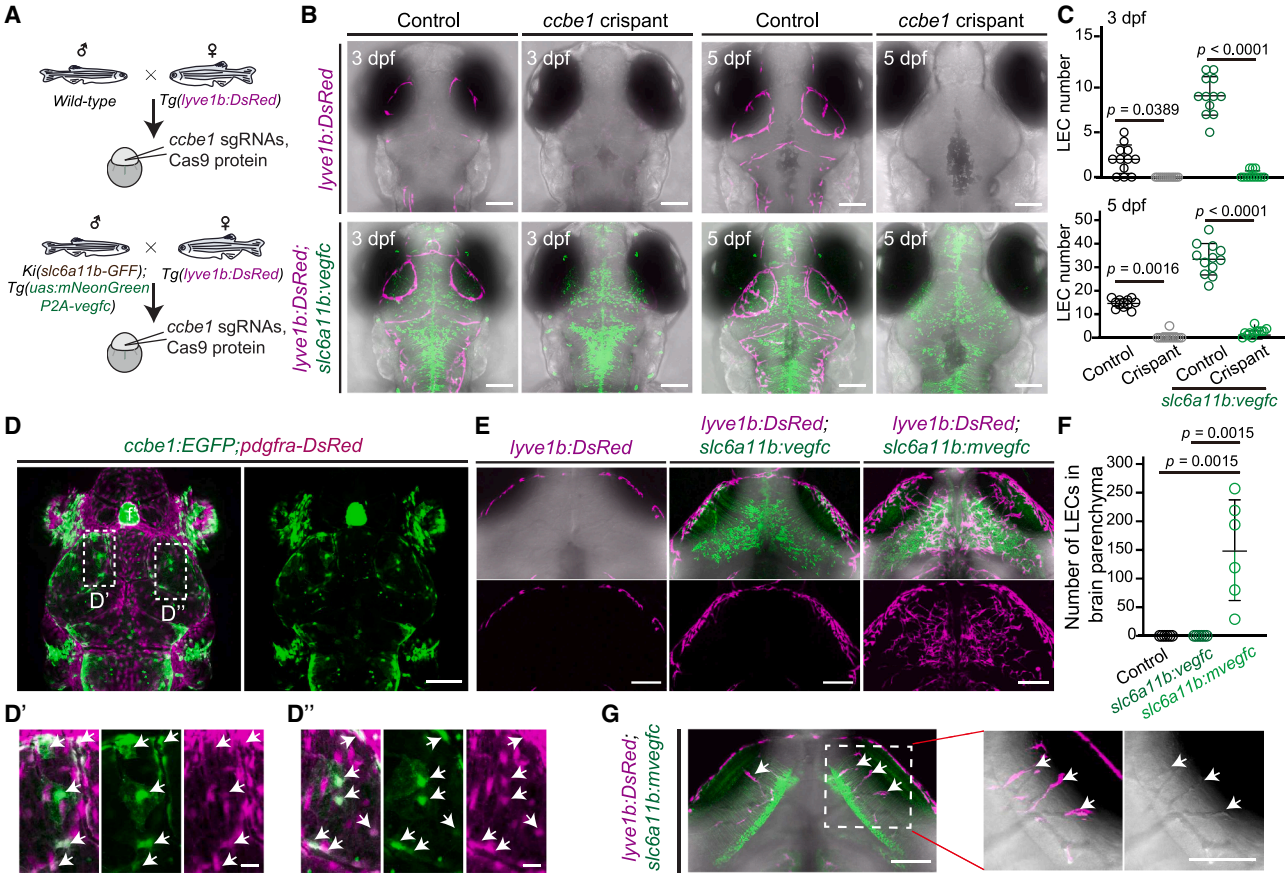

Figure 6. *ccbe1+* fibroblasts cooperate with *slc6a11b+* RAs in controlling muLEC patterning

(A–C) Effects of *ccbe1* knockout on muLEC development in normal larvae or larvae with *vegfc* overexpression in *slc6a11b+* RAs.

(A) Experimental design depicting the generation of *ccbe1* knockout crispants with background of *Tg(lyve1b:DsRed)* (top) or *Tg(lyve1b:DsRed);Ki(slc6a11b-GFF);Tg(uas:mNeonGreen-P2A-vegfc)* (abbreviated as *lyve1b:DsRed;slc6a11b:vegfc*) (bottom). Two *ccbe1* sgRNAs and Cas9 protein were co-injected in fertilized eggs.

(B and C) Representative images (B) and mean numbers (C) of muLECs on each side of the OT in 3- and 5-dpf *lyve1b:DsRed* larvae (top in B) and *lyve1b:DsRed; slc6a11b:vegfc* larvae (bottom in B). For the control groups, Cas9 protein only was injected.

(D) Representative images of co-labeling of *ccbe1+* cells and fibroblasts on the brain surface in a 6-dpf *Ki(ccbe1-GFF);Tg(uas:EGFP);Ki(pdgfra-DsRed)* (abbreviated as *ccbe1:EGFP;pdgfra-DsRed*) larva.

(D′ and D″) Enlarged images for the dashed boxes in (C), showing the co-localization (white arrows) of *ccbe1+* cells (green) with *pdgfra+* fibroblasts (red).

(E and F) Representative images of muLECs (E) and the mean number (F) of LECs inside of the brain parenchyma in the OT of *lyve1b:DsRed* control larvae (left in E), larvae with *slc6a11b+* cells expressing the coding sequence of the unprocessed full length Vegfc (*slc6a11b:vegfc*) (middle in E), and larvae with *slc6a11b+* cells expressing the coding sequence of processed mVegfc (*slc6a11b:mvegfc*) (right in E) at 9 dpf.

(G) z stacked image of the *slc6a11b:mvegfc* larva shown in the right in (E), showing lumenized LECs (white arrows) inside of the brain parenchyma.

Scale bars: 20 μm (D′ and D″), 100 μm (B, D, E, and G). Error bars represent SD. The *p* value was determined using the non-parametric one-tailed Kruskal-Wallis test with post hoc Dunnett's test (C and F). Data are represented as mean ± SD.

See also Figure S7.

compared with *vegfc*$^{fl/fl}$ controls (Figures 5G and 5H; see also Figures 1O and 1P). These results together indicate that neural activity regulates muLEC development through *vegfc* expression in *slc6a11b+* RAs.

ccbe1+ fibroblasts cooperate with *slc6a11b+* RAs in controlling muLEC patterning

Our results have shown that *slc6a11b+* RAs regulate muLEC development through the expression of *vegfc* in the brain. However, these glial cells are situated in the brain parenchyma, whereas muLECs locate at the leptomeninges. This raises the following interesting questions. How is the spatial localization of muLECs restricted to the brain surface? Alternatively, why can muLECs not invade the brain parenchyma?

CCBE1, an essential component for proteolytical processing of extracellular pro-Vegfc to its mature form, is known to function non-cell-autonomously for regulating lymphatics development.[47,50–52] By employing the crispant method,[53] which utilizes multiple synthetic short guidance RNAs (sgRNAs) with high cleavage efficiency to destroy the target gene, we found

Please cite this article in press as: Li et al., Neural-activity-regulated and glia-mediated control of brain lymphatic development, Cell (2025), https://doi.org/10.1016/j.cell.2025.04.008

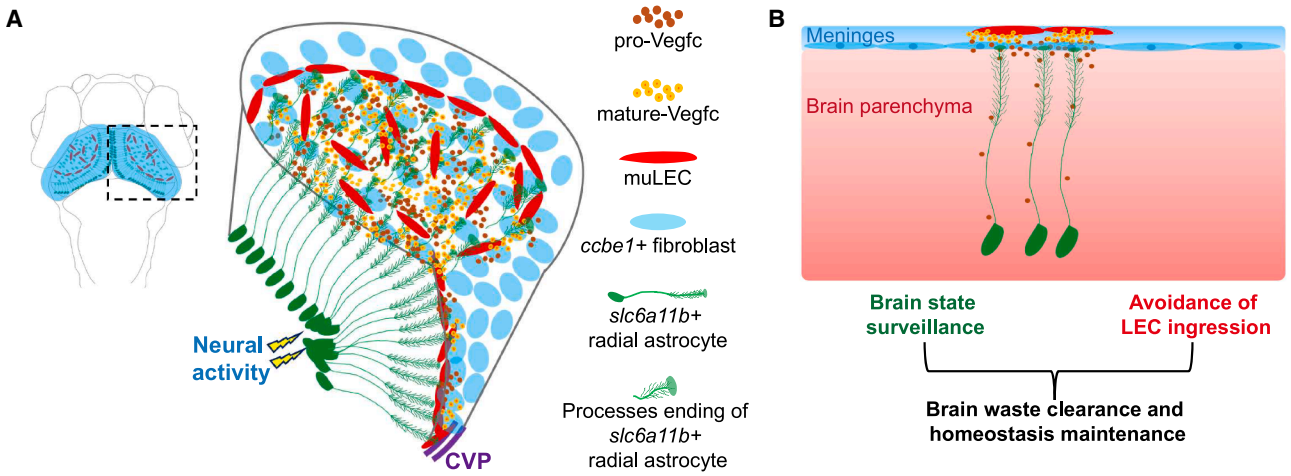

Figure 7. Working model for the brain control of muLEC development

(A) Diagram of three-dimensional view of the zebrafish brain illustrating that *slc6a11b+* RAs extend their processes to transport pro-Vegfc to the meninges, where *ccbe1+* fibroblasts collaborate with the RAs to convert pro-Vegfc into mature Vegfc (active form) at the interface between the brain parenchyma and the meningeal fibroblasts, restricting muLEC formation only at the brain surface.

(B) Diagram of the cross-sectional view showing the inter-tissue cooperation mechanism between *slc6a11b+* RAs inside of the brain and *ccbe1+* fibroblasts on the brain surface. This mechanism ensures the restricted distribution of muLECs to the brain surface without penetrating the interior, maintaining a balance between brain homeostasis and its immune surveillance needs while respecting the brain's unique anatomy.

that *ccbe1* knockout crispants exhibited the absence of muLECs, even when *vegfc* was overexpressed in *slc6a11b+* RAs (Figures 6A–6C). These results indicate that Ccbe1 is required for the control of muLEC development by *slc6a11b+* RAs.

We wondered how Ccbe1 helps *slc6a11b+* RAs in controlling muLEC development. By searching the scRNA-seq data, we found that *ccbe1* is expressed in fibroblasts (Figure S7A; see also Wang et al.[52]). We generated a *ccbe1* knockin line *Ki (ccbe1-GFF)* to examine its expression pattern (Figures S7B and S7C). Through imaging of *Ki(ccbe1-GFF);Tg(uas:EGFP);Ki (pdgfra-DsRed)* larvae, we found *ccbe1* expression in the fibroblasts localizing on the brain surface as well as in the trunk (Figures 6D and S7D). However, its expression was barely observed inside of the brain (Figure S7E). This suggests that the precise control of the muLEC pattern on the brain surface is likely achieved by cooperation between the *slc6a11b+* RAs and the *ccbe1+* fibroblasts.

Moreover, the overexpression of the mature form, but not the unprocessed form, of Vegfc in *slc6a11b+* RAs induced the ectopic growth of LECs into the brain (Figures 6E and 6F) and the formation of lumenized LECs within the brain parenchyma (Figure 6G). Taken together, these results indicate a precise control for Vegfc function that is mediated by two spatially separated cell types: *slc6a11b+* RAs inside the brain responsible for Vegfc production and *ccbe1+* fibroblasts on the brain surface responsible for Vegfc maturation. This strategy ensures the unique developmental patterning of muLECs, restricting them to the surface but not inside of the brain.

DISCUSSION

Here, we have unveiled a mechanism through which the brain controls the development of the muLEC, a vital component of zebrafish brain lymphatics. This control process is determined by a distinctive subpopulation of glia named as *slc6a11b+* RAs, which are the major cellular source of *vegfc* in the brain, and is modulated by neural activity. In cooperation with *ccbe1+* fibroblasts located outside of the brain, these specialized RAs play a pivotal role in shaping the unique developmental pattern of muLECs, specifically on the brain surface (Figure 7A). This discovery highlights an important interplay between the brain and its lymphatic system during development and also sheds light on our understanding of the diverse functions of different glia subtypes in maintaining brain homeostasis.

The traditional view of astrocytes as solely supporting cells in the CNS, originally considered homogeneous, has evolved significantly. Emerging studies unveiled regional diversity among astrocytes within different CNS regions in mammals.[54–56] In the adolescent mouse brain, distinct types of astrocytes with clear regionally restricted distributions have been identified.[57] Notably, the expression of *slc6a11* was found to be highly expressed in non-telencephalon astrocytes but absent in the cerebellum.[57] This expression pattern in mammals bears similarity to that of the *slc6a11b+* RAs we found in zebrafish, which primarily locate in the midbrain and hindbrain but not in the cerebellum (Video S5), suggesting that this type of RA may be evolutionarily conserved.

Our study indicates that *slc6a11b+* RAs can respond to neural activity with changeable *vegfc* expression, causing muLEC development tuned by neural activity. It is generally believed that glial activities are also affected by their intrinsic properties—like metabolic states and interactions with other cell types in the brain.[58,59] The neuropil region, primarily composed of neuronal and glial processes, serves as a hub where neural activities are intensely integrated and processed. Therefore, it is a region with a high concentration of metabolic wastes that

Please cite this article in press as: Li et al., Neural-activity-regulated and glia-mediated control of brain lymphatic development, Cell (2025), https://doi.org/10.1016/j.cell.2025.04.008

need to be efficiently removed to maintain proper physiological functionality.[58] Brain lymphatics, including the meningeal lymphatic vessels and muLECs, are important for clearing extracellular wastes from the brain parenchyma, thereby contributing to the overall homeostasis and immunosurveillance of the brain.[19–22,24,60–65] It makes sense for their function and development to be tightly regulated in a way that aligns with the brain's activities and needs.[66,67] Brain control of muLEC development ensures that these LECs are formed and maintained in a way that supports the proper functioning and health of the brain. The *slc6a11b+* RAs may act as vigilant sentinels and actively sense and respond to the brain's microenvironmental changes to regulate muLEC development, facilitating waste clearance in the brain. This intricate interplay between neural activity, glial activity, brain metabolism, and VEGFC production underscores the dynamic nature of *slc6a11b+* RAs' functions and their crucial role in brain lymphatics development.

It has been reported that *vegfc* transcription can be activated by oxidative stress.[68] Our GO term analysis revealed that *slc6a11b+* RAs exhibit the highest levels of oxidative phosphorylation and lipid metabolism (see Figures S4E and S4F). Furthermore, neural activity is known to associate with release of excess fatty acids in lipid particles that are transferred to glia for lipolysis through β-oxidation, a process that is critical for avoiding fatty acids toxicity during neural activity.[58] Therefore, it is likely that neural activity stimulates *slc6a11b+* RA activity to increase their lipid metabolism and energy production, leading to elevated oxidative phosphorylation levels in these cells. This could, in turn, regulate the transcription of *vegfc* in *slc6a11b+* RAs and enhance the development of muLECs on the brain surface.

To support its precise functions, the brain's priority is to maintain a stable and well-protected microenvironment, which may evolutionarily have led to the development of specialized mechanisms like the blood-brain barrier and brain lymphatics system.[12,69–71] The brain is sensitive to inflammation and immune responses, which can cause damage to its delicate neural connections and other structures.[63,70] Therefore, the absence of traditional lymphatics inside of the brain is an intriguing aspect of the anatomy and function of the brain.[20–22] LECs are present in the brain parenchyma only under conditions of diseases and injury.[72] This unique distribution pattern allows for the clearance of extracellular wastes and immune surveillance without invasive penetration of the brain tissue.[63] The expression of *vegfc* in *slc6a11b+* RAs and its processing and maturation by Ccbe1 secreted from fibroblasts on the brain surface cooperatively provide a localized and controlled mechanism for muLECs formation. The control of muLEC development involving different cell types in distinct locations should be a finely tuned mechanism that balances the microenvironmental homeostasis and immune surveillance needs of the brain, while respecting the brain's unique anatomy and avoiding unnecessary invasion into its parenchyma (Figure 7B).

Limitations of the study

First, how neural activity influences RA activity and the subsequent expression of *vegfc* is still unknown. In particular, it is not yet understood which types of neurons are involved, which receptors in RAs mediate the communication between neurons and the glia, and whether a key transcriptional factor plays a critical role in regulating *vegfc* expression. Future studies are needed to understand the cellular and molecular mechanisms underlying *vegfc* expression regulation in the glia. Second, it is unclear whether this glial regulation of leptomeningeal LEC development is conserved in mammals. Third, it is of great interest to examine whether such regulation functions in adults to help maintain muLECs under physiological conditions.

RESOURCE AVAILABILITY

Lead contact

Further information and requests for resources and reagents should be directed to, and will be fulfilled by, the lead contact, Jiu-lin Du (forestdu@ion.ac.cn).

Materials availability

Plasmids and fish lines generated in this study are available from the lead contact without restriction.

Data and code availability

- The raw sequence data reported in this paper have been deposited in the Genome Sequence Archive in National Genomics Data Center, China National Center for Bioinformation/Beijing Institute of Genomics, Chinese Academy of Sciences (GSA: CRA023422), which are publicly accessible at https://ngdc.cncb.ac.cn/gsa.
- This paper does not report any original code.
- Any additional information required to reanalyze the data reported in this work paper is available from the lead contact upon request.

ACKNOWLEDGMENTS

We are grateful to Dr. Didier Stainier for providing the *Tg(kdrl:EGFP)* line, Dr. David Traver for providing the *Tg(bactin2:loxP-BFP-stop-loxP-DsRed)* line, Dr. Koichi Kawakami for providing the *Tg(uas:EGFP)* and *Tg(uas:GCaMP6s)* lines, Dr. Drew Robson for providing the *Tg(elavl3:GCaMP6s)* line, Dr. Shanye Gu for providing the *lyve1b:DsRed* plasmid, Lin Zhu for establishing the electrical stimulation platform, Xinglan Liu from Shengjin Xu's lab for designing the probes and optimizing the protocol for the customized RNA FISH, and Dr. Chao Li and Yanqing Zhong at Single Cell Typing Platform of the Facility of Mapping Brain-wide Mesoscale Connectome for performing the RNA FISH experiment. This work was supported by the National Science and Technology Innovation 2030 Major Program (2021ZD0204500 and 2021ZD0204502 to J.-L.D.) and the National Key R&D Program (2019YFA0801603 to J.L.) of the Ministry of Science and Technology; Creative Research Groups (32321003 to J.-L.D.), General Program (82471286 to W.-J.D.), and the Young Scientist Fund (82001455 to W.D.) of the National Natural Science Foundation of China; the Shanghai Natural Science Foundation (22ZR1469700 to J.L.); the Shanghai Municipal Science and Technology Major Project (18JC1410100 to J.-L.D.); the Youth Innovation Promotion Association (to J.L.) and the Key Research Program of Frontier Sciences (QYZDYSSW-SMC028 to J.-L.D.) of the Chinese Academy of Sciences; and the SA-SIBS Scholarship Program (to J.L.).

AUTHOR CONTRIBUTIONS

J.L. and J.-L.D. conceived the study. J.-L.D. and J.L. supervised the project. J. L. and M.-J.L. designed the experiments, generated fish lines, performed the experiments, and analyzed the data. W.-J.D. conducted Ca^{2+} imaging and analysis. X.-L.P. and H.D. performed microinjection and confocal imaging. J. L. and H.-X.Z. performed the scRNA-seq experiments and analysis. J.L. and J.-L.D. wrote the manuscript, with inputs from M.-J.L., W.-J.D., X.-L.P., and H.-B.S.

DECLARATION OF INTERESTS

The authors declare no competing interests.

STAR★METHODS

Detailed methods are provided in the online version of this paper and include the following:

- KEY RESOURCES TABLE
- EXPERIMENTAL MODEL AND STUDY PARTICIPANT DETAILS
  - Zebrafish husbandry
  - Zebrafish lines
- METHOD DETAILS
  - Generation of transgenic zebrafish lines
  - CRISPR/Cas9-mediated knockin
  - CRISPR/Cas9-mediated knockout
  - Generation of a *vegfc*^{fl} allele
  - scRNA-seq library preparation and analysis
  - Multiplexed Fluorescence In Situ Hybridization (FISH) using a customized Hybridization Chain Reaction (HCR) protocol
  - Transient injection for mosaic labeling of the glia
  - Chemical treatment
  - In vivo confocal imaging of cell morphology and Ca^{2+} activity
  - Analysis of Ca^{2+} activity
  - Visual stimulation by moving bars and flashes
  - Electrical stimulation
  - Optogenetic activation
- QUANTIFICATION AND STATISTICAL ANALYSIS
  - Statistics
  - Software

SUPPLEMENTAL INFORMATION

Supplemental information can be found online at https://doi.org/10.1016/j.cell.2025.04.008.

Received: October 30, 2024
Revised: January 28, 2025
Accepted: April 3, 2025
Published: April 30, 2025

REFERENCES

1. Schiller, M., Ben-Shaanan, T.L., and Rolls, A. (2021). Neuronal regulation of immunity: why, how and where? Nat. Rev. Immunol. *21*, 20–36. https://doi.org/10.1038/s41577-020-0387-1.
2. Jin, H., Li, M., Jeong, E., Castro-Martinez, F., and Zuker, C.S. (2024). A body-brain circuit that regulates body inflammatory responses. Nature *630*, 695–703. https://doi.org/10.1038/s41586-024-07469-y.
3. Ben-Shaanan, T.L., Azulay-Debby, H., Dubovik, T., Starosvetsky, E., Korin, B., Schiller, M., Green, N.L., Admon, Y., Hakim, F., Shen-Orr, S.S., et al. (2016). Activation of the reward system boosts innate and adaptive immunity. Nat. Med. *22*, 940–944. https://doi.org/10.1038/nm.4133.
4. Zhang, X., Lei, B., Yuan, Y., Zhang, L., Hu, L., Jin, S., Kang, B., Liao, X., Sun, W., Xu, F., et al. (2020). Brain control of humoral immune responses amenable to behavioural modulation. Nature *581*, 204–208. https://doi.org/10.1038/s41586-020-2235-7.
5. Cardoso, F., Klein Wolterink, R.G.J., Godinho-Silva, C., Domingues, R.G., Ribeiro, H., da Silva, J.A., Mahú, I., Domingos, A.I., and Veiga-Fernandes, H. (2021). Neuro-mesenchymal units control ILC2 and obesity via a brain-adipose circuit. Nature *597*, 410–414. https://doi.org/10.1038/s41586-021-03830-7.
6. Koren, T., Yifa, R., Amer, M., Krot, M., Boshnak, N., Ben-Shaanan, T.L., Azulay-Debby, H., Zalayat, I., Avishai, E., Hajjo, H., et al. (2021). Insular cortex neurons encode and retrieve specific immune responses. Cell *184*, 5902–5915.e17. https://doi.org/10.1016/j.cell.2021.10.013.
7. Poller, W.C., Downey, J., Mooslechner, A.A., Khan, N., Li, L., Chan, C.T., McAlpine, C.S., Xu, C., Kahles, F., He, S., et al. (2022). Brain motor and fear circuits regulate leukocytes during acute stress. Nature *607*, 578–584. https://doi.org/10.1038/s41586-022-04890-z.
8. Yang, D., Jacobson, A., Meerschaert, K.A., Sifakis, J.J., Wu, M., Chen, X., Yang, T., Zhou, Y., Anekal, P.V., Rucker, R.A., et al. (2022). Nociceptor neurons direct goblet cells via a CGRP-RAMP1 axis to drive mucus production and gut barrier protection. Cell *185*, 4190–4205.e25. https://doi.org/10.1016/j.cell.2022.09.024.
9. Zhu, Y., Meerschaert, K.A., Galvan-Pena, S., Bin, N.R., Yang, D., Basu, H., Kawamoto, R., Shalaby, A., Liberles, S.D., Mathis, D., et al. (2024). A chemogenetic screen reveals that Trpv1-expressing neurons control regulatory T cells in the gut. Science *385*, eadk1679. https://doi.org/10.1126/science.adk1679.
10. Borovikova, L.V., Ivanova, S., Zhang, M., Yang, H., Botchkina, G.I., Watkins, L.R., Wang, H., Abumrad, N., Eaton, J.W., and Tracey, K.J. (2000). Vagus nerve stimulation attenuates the systemic inflammatory response to endotoxin. Nature *405*, 458–462. https://doi.org/10.1038/35013070.
11. Koopman, F.A., Chavan, S.S., Miljko, S., Grazio, S., Sokolovic, S., Schuurman, P.R., Mehta, A.D., Levine, Y.A., Faltys, M., Zitnik, R., et al. (2016). Vagus nerve stimulation inhibits cytokine production and attenuates disease severity in rheumatoid arthritis. Proc. Natl. Acad. Sci. USA *113*, 8284–8289. https://doi.org/10.1073/pnas.1605635113.
12. Castellani, G., Croese, T., Peralta Ramos, J.M., and Schwartz, M. (2023). Transforming the understanding of brain immunity. Science *380*, eabo7649. https://doi.org/10.1126/science.abo7649.
13. Koren, T., and Rolls, A. (2022). Immunoception: Defining brain-regulated immunity. Neuron *110*, 3425–3428. https://doi.org/10.1016/j.neuron.2022.10.016.
14. Bower, N.I., Koltowska, K., Pichol-Thievend, C., Virshup, I., Paterson, S., Lagendijk, A.K., Wang, W., Lindsey, B.W., Bent, S.J., Baek, S., et al. (2017). Mural lymphatic endothelial cells regulate meningeal angiogenesis in the zebrafish. Nat. Neurosci. *20*, 774–783. https://doi.org/10.1038/nn.4558.
15. Venero Galanternik, M., Castranova, D., Gore, A.V., Blewett, N.H., Jung, H.M., Stratman, A.N., Kirby, M.R., Iben, J., Miller, M.F., Kawakami, K., et al. (2017). A novel perivascular cell population in the zebrafish brain. eLife *6*, e24369. https://doi.org/10.7554/eLife.24369.
16. van Lessen, M., Shibata-Germanos, S., van Impel, A., Hawkins, T.A., Rihel, J., and Schulte-Merker, S. (2017). Intracellular uptake of macromolecules by brain lymphatic endothelial cells during zebrafish embryonic development. eLife *6*, e25932. https://doi.org/10.7554/eLife.25932.
17. Siret, C., van Lessen, M., Bavais, J., Jeong, H.W., Reddy Samawar, S.K., Kapupara, K., Wang, S., Simic, M., de Fabritus, L., Tchoghandjian, A., et al. (2022). Deciphering the heterogeneity of the Lyve1(+) perivascular macrophages in the mouse brain. Nat. Commun. *13*, 7366. https://doi.org/10.1038/s41467-022-35166-9.
18. Shibata-Germanos, S., Goodman, J.R., Grieg, A., Trivedi, C.A., Benson, B.C., Foti, S.C., Faro, A., Castellan, R.F.P., Correra, R.M., Barber, M., et al. (2020). Structural and functional conservation of non-lumenized lymphatic endothelial cells in the mammalian leptomeninges. Acta Neuropathol. *139*, 383–401. https://doi.org/10.1007/s00401-019-02091-z.
19. Castranova, D., Samasa, B., Venero Galanternik, M., Jung, H.M., Pham, V.N., and Weinstein, B.M. (2021). Live Imaging of Intracranial Lymphatics in the Zebrafish. Circ. Res. *128*, 42–58. https://doi.org/10.1161/CIRCRESAHA.120.317372.

20. Aspelund, A., Antila, S., Proulx, S.T., Karlsen, T.V., Karaman, S., Detmar, M., Wiig, H., and Alitalo, K. (2015). A dural lymphatic vascular system that drains brain interstitial fluid and macromolecules. J. Exp. Med. *212*, 991–999. https://doi.org/10.1084/jem.20142290.

21. Louveau, A., Smirnov, I., Keyes, T.J., Eccles, J.D., Rouhani, S.J., Peske, J. D., Derecki, N.C., Castle, D., Mandell, J.W., Lee, K.S., et al. (2015). Structural and functional features of central nervous system lymphatic vessels. Nature *523*, 337–341. https://doi.org/10.1038/nature14432.

22. Suárez, I., and Schulte-Merker, S. (2021). Cells with Many Talents: Lymphatic Endothelial Cells in the Brain Meninges. Cells *10*, 799. https://doi.org/10.3390/cells10040799.

23. Nicenboim, J., Malkinson, G., Lupo, T., Asaf, L., Sela, Y., Mayseless, O., Gibbs-Bar, L., Senderovich, N., Hashimshony, T., Shin, M., et al. (2015). Lymphatic vessels arise from specialized angioblasts within a venous niche. Nature *522*, 56–61-U100. https://doi.org/10.1038/nature14425.

24. Huisman, Y., Uphoff, K., Berger, M., Dobrindt, U., Schelhaas, M., Zobel, T., Bussmann, J., van Impel, A., and Schulte-Merker, S. (2022). Meningeal lymphatic endothelial cells fulfill scavenger endothelial cell function and cooperate with microglia in waste removal from the brain. Glia *70*, 35–49. https://doi.org/10.1002/glia.24081.

25. Robles, E., Laurell, E., and Baier, H. (2014). The retinal projectome reveals brain-area-specific visual representations generated by ganglion cell diversity. Curr. Biol. *24*, 2085–2096. https://doi.org/10.1016/j.cub.2014.07.080.

26. Panula, P., Chen, Y.C., Priyadarshini, M., Kudo, H., Semenova, S., Sundvik, M., and Sallinen, V. (2010). The comparative neuroanatomy and neurochemistry of zebrafish CNS systems of relevance to human neuropsychiatric diseases. Neurobiol. Dis. *40*, 46–57. https://doi.org/10.1016/j.nbd.2010.05.010.

27. Jurisch-Yaksi, N., Yaksi, E., and Kizil, C. (2020). Radial glia in the zebrafish brain: Functional, structural, and physiological comparison with the mammalian glia. Glia *68*, 2451–2470. https://doi.org/10.1002/glia.23849.

28. Quiñonez-Silvero, C., Hübner, K., and Herzog, W. (2020). Development of the brain vasculature and the blood-brain barrier in zebrafish. Dev. Biol. *457*, 181–190. https://doi.org/10.1016/j.ydbio.2019.03.005.

29. Karkkainen, M.J., Haiko, P., Sainio, K., Partanen, J., Taipale, J., Petrova, T. V., Jeltsch, M., Jackson, D.G., Talikka, M., Rauvala, H., et al. (2004). Vascular endothelial growth factor C is required for sprouting of the first lymphatic vessels from embryonic veins. Nat. Immunol. *5*, 74–80. https://doi.org/10.1038/ni1013.

30. Ober, E.A., Olofsson, B., Mäkinen, T., Jin, S.W., Shoji, W., Koh, G.Y., Alitalo, K., and Stainier, D.Y.R. (2004). Vegfc is required for vascular development and endoderm morphogenesis in zebrafish. EMBO Rep. *5*, 78–84. https://doi.org/10.1038/sj.embor.7400047.

31. Okuda, K.S., Astin, J.W., Misa, J.P., Flores, M.V., Crosier, K.E., and Crosier, P.S. (2012). lyve1 expression reveals novel lymphatic vessels and new mechanisms for lymphatic vessel development in zebrafish. Development *139*, 2381–2391. https://doi.org/10.1242/dev.077701.

32. Beiter, R.M., Rivet-Noor, C., Merchak, A.R., Bai, R., Johanson, D.M., Slogar, E., Sol-Church, K., Overall, C.C., and Gaultier, A. (2022). Evidence for oligodendrocyte progenitor cell heterogeneity in the adult mouse brain. Sci. Rep. *12*, 12921. https://doi.org/10.1038/s41598-022-17081-7.

33. Zhang, B.B., Yao, Y.Y., Zhang, H.F., Kawakami, K., and Du, J.L. (2017). Left Habenula Mediates Light-Preference Behavior in Zebrafish via an Asymmetrical Visual Pathway. Neuron *93*, 914–928.e4. https://doi.org/10.1016/j.neuron.2017.01.011.

34. Barabási, D.L., Schuhknecht, G.F.P., and Engert, F. (2024). Functional neuronal circuits emerge in the absence of developmental activity. Nat. Commun. *15*, 364. https://doi.org/10.1038/s41467-023-44681-2.

35. Leyden, C., Brüggemann, T., Debinski, F., Simacek, C.A., Dehmelt, F.A., and Arrenberg, A.B. (2022). Efficacy of Tricaine (MS-222) and Hypothermia as Anesthetic Agents for Blocking Sensorimotor Responses in Larval Zebrafish. Front. Vet. Sci. *9*, 864573. https://doi.org/10.3389/fvets.2022.864573.

36. Albensi, B.C., Oliver, D.R., Toupin, J., and Odero, G. (2007). Electrical stimulation protocols for hippocampal synaptic plasticity and neuronal hyper-excitability: are they effective or relevant? Exp. Neurol. *204*, 1–13. https://doi.org/10.1016/j.expneurol.2006.12.009.

37. Bower, N.I., Vogrin, A.J., Le Guen, L., Chen, H., Stacker, S.A., Achen, M. G., and Hogan, B.M. (2017). Vegfd modulates both angiogenesis and lymphangiogenesis during zebrafish embryonic development. Development *144*, 507–518. https://doi.org/10.1242/dev.146969.

38. Antila, S., Karaman, S., Nurmi, H., Airavaara, M., Voutilainen, M.H., Mathivet, T., Chilov, D., Li, Z.L., Koppinen, T., Park, J.H., et al. (2017). Development and plasticity of meningeal lymphatic vessels. J. Exp. Med. *214*, 3645–3667. https://doi.org/10.1084/jem.20170391.

39. Shin, M., Male, I., Beane, T.J., Villefranc, J.A., Kok, F.O., Zhu, L.J., and Lawson, N.D. (2017). Correction: Vegfc acts through ERK to induce sprouting and differentiation of trunk lymphatic progenitors. Development *144*, 531. https://doi.org/10.1242/dev.148569.

40. Jerafi-Vider, A., Bassi, I., Moshe, N., Tevet, Y., Hen, G., Splittstoesser, D., Shin, M., Lawson, N.D., and Yaniv, K. (2021). VEGFC/FLT4-induced cell-cycle arrest mediates sprouting and differentiation of venous and lymphatic endothelial cells. Cell Rep. *35*, 109255. https://doi.org/10.1016/j.celrep.2021.109255.

41. Li, J., Zhang, B.B., Ren, Y.G., Gu, S.Y., Xiang, Y.H., and Du, J.L. (2015). Intron targeting-mediated and endogenous gene integrity-maintaining knockin in zebrafish using the CRISPR/Cas9 system. Cell Res. *25*, 634–637. https://doi.org/10.1038/cr.2015.43.

42. Zi, H., Peng, X., Du, J., and Li, J. (2025). Protocol for generating a pericyte reporter zebrafish line Ki(pdgfrb-P2A-GAL4-VP16) using a CRISPR-Cas9-mediated knockin technique. Star Protoc. *6*, 103490. https://doi.org/10.1016/j.xpro.2024.103490.

43. Choi, H.M.T., Schwarzkopf, M., Fornace, M.E., Acharya, A., Artavanis, G., Stegmaier, J., Cunha, A., and Pierce, N.A. (2018). Third-generation hybridization chain reaction: multiplexed, quantitative, sensitive, versatile, robust. Development *145*, dev165753. https://doi.org/10.1242/dev.165753.

44. Yang, Y., Vidensky, S., Jin, L., Jie, C., Lorenzini, I., Frankl, M., and Rothstein, J.D. (2011). Molecular comparison of GLT1+ and ALDH1L1+ astrocytes in vivo in astroglial reporter mice. Glia *59*, 200–207. https://doi.org/10.1002/glia.21089.

45. Yu, X., Taylor, A.M.W., Nagai, J., Golshani, P., Evans, C.J., Coppola, G., and Khakh, B.S. (2018). Reducing Astrocyte Calcium Signaling In Vivo Alters Striatal Microcircuits and Causes Repetitive Behavior. Neuron *99*, 1170–1187.e9. https://doi.org/10.1016/j.neuron.2018.08.015.

46. Sharrock, A.V., Mulligan, T.S., Hall, K.R., Williams, E.M., White, D.T., Zhang, L., Emmerich, K., Matthews, F., Nimmagadda, S., Washington, S., et al. (2022). NTR 2.0: a rationally engineered prodrug-converting enzyme with substantially enhanced efficacy for targeted cell ablation. Nat. Methods *19*, 205–215. https://doi.org/10.1038/s41592-021-01364-4.

47. Le Guen, L., Karpanen, T., Schulte, D., Harris, N.C., Koltowska, K., Roukens, G., Bower, N.I., van Impel, A., Stacker, S.A., Achen, M.G., et al. (2014). Ccbe1 regulates Vegfc-mediated induction of Vegfr3 signaling during embryonic lymphangiogenesis. Development *141*, 1239–1249. https://doi.org/10.1242/dev.100495.

48. Li, J., Li, H.Y., Gu, S.Y., Zi, H.X., Jiang, L., and Du, J.L. (2020). One-step generation of zebrafish carrying a conditional knockout-knockin visible switch via CRISPR/Cas9-mediated intron targeting. Sci. China Life Sci. *63*, 59–67. https://doi.org/10.1007/s11427-019-1607-9.

49. Kobayashi, I., Kobayashi-Sun, J., Kim, A.D., Pouget, C., Fujita, N., Suda, T., and Traver, D. (2014). Jam1a-Jam2a interactions regulate haematopoietic stem cell fate through Notch signalling. Nature *512*, 319–323. https://doi.org/10.1038/nature13623.

50. Hogan, B.M., Bos, F.L., Bussmann, J., Witte, M., Chi, N.C., Duckers, H.J., and Schulte-Merker, S. (2009). Ccbe1 is required for embryonic lymphangiogenesis and venous sprouting. Nat. Genet. *41*, 396–398. https://doi.org/10.1038/ng.321.

51. Alders, M., Hogan, B.M., Gjini, E., Salehi, F., Al-Gazali, L., Hennekam, E.A., Holmberg, E.E., Mannens, M.M.A.M., Mulder, M.F., Offerhaus, G.J.A., et al. (2009). Mutations in CCBE1 cause generalized lymph vessel dysplasia in humans. Nat. Genet. *41*, 1272–1274. https://doi.org/10.1038/ng.484.

52. Wang, G., Muhl, L., Padberg, Y., Dupont, L., Peterson-Maduro, J., Stehling, M., le Noble, F., Colige, A., Betsholtz, C., Schulte-Merker, S., et al. (2020). Specific fibroblast subpopulations and neuronal structures provide local sources of Vegfc-processing components during zebrafish lymphangiogenesis. Nat. Commun. *11*, 2724. https://doi.org/10.1038/s41467-020-16552-7.

53. Kroll, F., Powell, G.T., Ghosh, M., Gestri, G., Antinucci, P., Hearn, T.J., Tunbak, H., Lim, S., Dennis, H.W., Fernandez, J.M., et al. (2021). A simple and effective F0 knockout method for rapid screening of behaviour and other complex phenotypes. eLife *10*, e59683. https://doi.org/10.7554/eLife.59683.

54. Chai, H., Diaz-Castro, B., Shigetomi, E., Monte, E., Octeau, J.C., Yu, X., Cohn, W., Rajendran, P.S., Vondriska, T.M., Whitelegge, J.P., et al. (2017). Neural Circuit-Specialized Astrocytes: Transcriptomic, Proteomic, Morphological, and Functional Evidence. Neuron *95*, 531–549.e9. https://doi.org/10.1016/j.neuron.2017.06.029.

55. Batiuk, M.Y., Martirosyan, A., Wahis, J., de Vin, F., Marneffe, C., Kusserow, C., Koeppen, J., Viana, J.F., Oliveira, J.F., Voet, T., et al. (2020). Identification of region-specific astrocyte subtypes at single cell resolution. Nat. Commun. *11*, 1220. https://doi.org/10.1038/s41467-019-14198-8.

56. Huang, A.Y.S., Woo, J., Sardar, D., Lozzi, B., Bosquez Huerta, N.A., Lin, C.J., Felice, D., Jain, A., Paulucci-Holthauzen, A., and Deneen, B. (2020). Region-Specific Transcriptional Control of Astrocyte Function Oversees Local Circuit Activities. Neuron *106*, 992–1008.e9. https://doi.org/10.1016/j.neuron.2020.03.025.

57. Zeisel, A., Hochgerner, H., Lönnerberg, P., Johnsson, A., Memic, F., van der Zwan, J., Häring, M., Braun, E., Borm, L.E., La Manno, G., et al. (2018). Molecular Architecture of the Mouse Nervous System. Cell *174*, 999–1014.e22. https://doi.org/10.1016/j.cell.2018.06.021.

58. Ioannou, M.S., Jackson, J., Sheu, S.H., Chang, C.L., Weigel, A.V., Liu, H., Pasolli, H.A., Xu, C.S., Pang, S., Matthies, D., et al. (2019). Neuron-Astrocyte Metabolic Coupling Protects against Activity-Induced Fatty Acid Toxicity. Cell *177*, 1522–1535.e14. https://doi.org/10.1016/j.cell.2019.04.001.

59. Theparambil, S.M., Kopach, O., Braga, A., Nizari, S., Hosford, P.S., Sagi-Kiss, V., Hadjihambi, A., Konstantinou, C., Esteras, N., Gutierrez Del Arroyo, A., et al. (2024). Adenosine signalling to astrocytes coordinates brain metabolism and function. Nature *632*, 139–146. https://doi.org/10.1038/s41586-024-07611-w.

60. Song, E., Mao, T., Dong, H., Boisserand, L.S.B., Antila, S., Bosenberg, M., Alitalo, K., Thomas, J.L., and Iwasaki, A. (2020). VEGF-C-driven lymphatic drainage enables immunosurveillance of brain tumours. Nature *577*, 689–694. https://doi.org/10.1038/s41586-019-1912-x.

61. Hu, X., Deng, Q., Ma, L., Li, Q., Chen, Y., Liao, Y., Zhou, F., Zhang, C., Shao, L., Feng, J., et al. (2020). Meningeal lymphatic vessels regulate brain tumor drainage and immunity. Cell Res. *30*, 229–243. https://doi.org/10.1038/s41422-020-0287-8.

62. Da Mesquita, S., Fu, Z., and Kipnis, J. (2018). The Meningeal Lymphatic System: A New Player in Neurophysiology. Neuron *100*, 375–388. https://doi.org/10.1016/j.neuron.2018.09.022.

63. Alves de Lima, K., Rustenhoven, J., and Kipnis, J. (2020). Meningeal Immunity and Its Function in Maintenance of the Central Nervous System in Health and Disease. Annu. Rev. Immunol. *38*, 597–620. https://doi.org/10.1146/annurev-immunol-102319-103410.

64. Oliver, G., Kipnis, J., Randolph, G.J., and Harvey, N.L. (2020). The Lymphatic Vasculature in the 21(st) Century: Novel Functional Roles in Homeostasis and Disease. Cell *182*, 270–296. https://doi.org/10.1016/j.cell.2020.06.039.

65. Salvador, A.F.M., Abduljawad, N., and Kipnis, J. (2024). Meningeal Lymphatics in Central Nervous System Diseases. Annu. Rev. Neurosci. *47*, 323–344. https://doi.org/10.1146/annurev-neuro-113023-103045.

66. Jiang-Xie, L.F., Drieu, A., Bhasiin, K., Quintero, D., Smirnov, I., and Kipnis, J. (2024). Neuronal dynamics direct cerebrospinal fluid perfusion and brain clearance. Nature *627*, 157–164. https://doi.org/10.1038/s41586-024-07108-6.

67. Murdock, M.H., Yang, C.Y., Sun, N., Pao, P.C., Blanco-Duque, C., Kahn, M.C., Kim, T., Lavoie, N.S., Victor, M.B., Islam, M.R., et al. (2024). Multisensory gamma stimulation promotes glymphatic clearance of amyloid. Nature *627*, 149–156. https://doi.org/10.1038/s41586-024-07132-6.

68. Cohen, B., Addadi, Y., Sapoznik, S., Meir, G., Kalchenko, V., Harmelin, A., Ben-Dor, S., and Neeman, M. (2009). Transcriptional regulation of vascular endothelial growth factor C by oxidative and thermal stress is mediated by lens epithelium-derived growth factor/p75. Neoplasia *11*, 921–933. https://doi.org/10.1593/neo.09636.

69. Ribatti, D., Nico, B., Crivellato, E., and Artico, M. (2006). Development of the blood-brain barrier: a historical point of view. Anat. Rec. B New Anat. *289*, 3–8. https://doi.org/10.1002/ar.b.20087.

70. Rustenhoven, J., and Kipnis, J. (2019). Bypassing the blood-brain barrier. Science *366*, 1448–1449. https://doi.org/10.1126/science.aay0479.

71. Schwartz, M., Abellanas, M.A., Tsitsou-Kampeli, A., and Suzzi, S. (2022). The brain-immune ecosystem: Implications for immunotherapy in defeating neurodegenerative diseases. Neuron *110*, 3421–3424. https://doi.org/10.1016/j.neuron.2022.09.007.

72. Chen, J., He, J., Ni, R., Yang, Q., Zhang, Y., and Luo, L. (2019). Cerebrovascular Injuries Induce Lymphatic Invasion into Brain Parenchyma to Guide Vascular Regeneration in Zebrafish. Dev. Cell *49*, 697–710.e5. https://doi.org/10.1016/j.devcel.2019.03.022.

73. Kim, D.H., Kim, J., Marques, J.C., Grama, A., Hildebrand, D.G.C., Gu, W.C., Li, J.M., and Robson, D.N. (2017). Pan-neuronal calcium imaging with cellular resolution in freely swimming zebrafish. Nat. Methods *14*, 1107–1114. https://doi.org/10.1038/Nmeth.4429.

74. Feng, J., Zhang, C., Lischinsky, J.E., Jing, M., Zhou, J., Wang, H., Zhang, Y., Dong, A., Wu, Z., Wu, H., et al. (2019). A Genetically Encoded Fluorescent Sensor for Rapid and Specific In Vivo Detection of Norepinephrine. Neuron *102*, 745–761.e8. https://doi.org/10.1016/j.neuron.2019.02.037.

75. Jiao, Z.F., Shang, C.F., Wang, Y.F., Yang, Z., Yang, C., Li, F.N., Xie, J.Z., Pan, J.W., Fu, L., and Du, J.L. (2018). All-optical imaging and manipulation of whole-brain neuronal activities in behaving larval zebrafish. Biomed. Opt. Express *9*, 6154–6169. https://doi.org/10.1364/BOE.9.006154.

76. Chen, T., Deng, Q., Lin, K., Zheng, X., Wang, X., Zhong, Y., Ning, X., Li, Y., Xu, F., Du, J., et al. (2024). An applicable and efficient retrograde monosynaptic circuit mapping tool for larval zebrafish. eLife. https://doi.org/10.7554/eLife.100880.1.

77. Asakawa, K., Suster, M.L., Mizusawa, K., Nagayoshi, S., Kotani, T., Urasaki, A., Kishimoto, Y., Hibi, M., and Kawakami, K. (2008). Genetic dissection of neural circuits by Tol2 transposon-mediated Gal4 gene and enhancer trapping in zebrafish. Proc. Natl. Acad. Sci. USA *105*, 1255–1260. https://doi.org/10.1073/pnas.0704963105.

78. Muto, A., Lal, P., Ailani, D., Abe, G., Itoh, M., and Kawakami, K. (2017). Activation of the hypothalamic feeding centre upon visual prey detection. Nat. Commun. *8*, 15029. https://doi.org/10.1038/ncomms15029.

79. Jin, S.W., Beis, D., Mitchell, T., Chen, J.N., and Stainier, D.Y.R. (2005). Cellular and molecular analyses of vascular tube and lumen formation in zebrafish. Development *132*, 5199–5209. https://doi.org/10.1242/dev.02087.

80. Lister, J.A., Robertson, C.P., Lepage, T., Johnson, S.L., and Raible, D.W. (1999). nacre encodes a zebrafish microphthalmia-related protein that regulates neural-crest-derived pigment cell fate. Development *126*, 3757–3767. https://doi.org/10.1242/dev.126.17.3757.

81. Zi, H., Peng, X., Cao, J., Xie, T., Liu, T., Li, H., Bu, J., Du, J., and Li, J. (2024). Piezo1-dependent regulation of pericyte proliferation by blood flow during brain vascular development. Cell Rep. *43*, 113652. https://doi.org/10.1016/j.celrep.2023.113652.

82. Urasaki, A., and Kawakami, K. (2009). Analysis of genes and genome by the tol2-mediated gene and enhancer trap methods. Methods Mol. Biol. *546*, 85–102. https://doi.org/10.1007/978-1-60327-977-2_6.

83. Zhao, D., Jones, J.L., Gasperini, R.J., Charlesworth, J.C., Liu, G.S., and Burdon, K.P. (2021). Rapid and efficient cataract gene evaluation in F0 zebrafish using CRISPR-Cas9 ribonucleoprotein complexes. Methods *194*, 37–47. https://doi.org/10.1016/j.ymeth.2020.12.004.

Please cite this article in press as: Li et al., Neural-activity-regulated and glia-mediated control of brain lymphatic development, Cell (2025), https://doi.org/10.1016/j.cell.2025.04.008

STAR★METHODS

KEY RESOURCES TABLE

REAGENT or RESOURCE	SOURCE	IDENTIFIER
Chemicals, peptides, and recombinant proteins		
Proteinase K (for genome extraction)	Tiangen	RT403
Proteinase K (for FISH)	Thermo Scientific	EO0491
T4 DNA Ligase	Takara	2011A
Tricaine/MS-222	Sigma	E10521
Low melting point agarose	Invitrogen	827503
MTZ	Sigma	M1547
4% PFA, RNase free	Bioss	C2055
PBS (1X) pH7.4	Gibco	10010-031
Ethanol	General-reagent	G73537A
DEPC-treated water	Sangon	B501005
SSC (20X), RNase-free	Invitrogen	AM9770
Triton X-100	Sigma	T8787
Tween 20	Abcam	ab128987
Critical commercial assays		
PrimeSTAR MAX DNA Polymerase	Takara	R045Q
TIANprep Rapid Mini Plasmid Kit	Tiangen	DP105-03
QIAquick Gel Extraction Kit	QIAGEN	28706
2x Es Taq Master Mix	CWBIO	CW0690H
Experimental models: organisms/strains		
Zebrafish *Ki(vegfc-GFF)*	This paper	Jiu-Lin Du Lab
Zebrafish *Ki(slc6a11b-GFF)*	This paper	Jiu-Lin Du Lab
Zebrafish *Ki(vegfd-GFF)*	This paper	Jiu-Lin Du Lab
Zebrafish *Ki(pdgfra-GFF)*	This paper	Jiu-Lin Du Lab
Zebrafish *Ki(ccbe1-GFF)*	This paper	Jiu-Lin Du Lab
Zebrafish *Ki(pdgfra-DsRed)*	This paper	Jiu-Lin Du Lab
Zebrafish *Tg(lyve1b:DsRed)*	This paper	Jiu-Lin Du Lab
Zebrafish *Tg(lyve1b:DsRed-P2A-nGFP)*	This paper	Jiu-Lin Du Lab
Zebrafish *Tg(elavl3:GCaMP6s)*	Kim et al.[73]	D. Robson Lab
Zebrafish *Tg(elavl3:NES-jRGECO1a)*	Feng et al.[74]	Jiu-Lin Du Lab
Zebrafish *Tg(elavl3:ChrimsonR-tdTomato)*	Jiao et al.[75]	Jiu-Lin Du Lab
Zebrafish *Tg(gfap:NTR-mCherry)*	This paper	Jiu-Lin Du Lab
Zebrafish *Tg(2×en.cpce:tdTomato-CAAX)*	Chen et al.[76]	Jiu-Lin Du Lab
Zebrafish *Tg(uas:mNeonGreen-P2A-mvegfc)*	This paper	Jiu-Lin Du Lab
Zebrafish *Tg(uas:NTR2.0-P2A-EGFP)*	This paper	Jiu-Lin Du Lab
Zebrafish *Tg(uas:mNeonGreen-P2A-sflt4)*	This paper	Jiu-Lin Du Lab
Zebrafish *Tg(uas:mNeonGreen-P2A-Cre)*	This paper	Jiu-Lin Du Lab
Zebrafish *Tg(uas:CoChR-EGFP-P2A-H2B-mScarlet)*	This paper	Jiu-Lin Du Lab
Zebrafish *vegfc*^{fl}	This paper	Jiu-Lin Du Lab
Zebrafish *vegfc*$^{-/-}$	This paper	Jiu-Lin Du Lab
Zebrafish *vegfd*$^{-/-}$	This paper	Jiu-Lin Du Lab
Zebrafish *Tg(uas:EGFP)*^{nkuasgfp1a}	Asakawa et al.[77]	K. Kawakami Lab
Zebrafish *Tg(uas:GCaMP6s)*	Muto et al.[78]	K. Kawakami Lab
Zebrafish *Tg(kdrl:EGFP)*^{s843}	Jin et al.[79]	D. Stainier Lab

(*Continued on next page*)

Please cite this article in press as: Li et al., Neural-activity-regulated and glia-mediated control of brain lymphatic development, Cell (2025), https://doi.org/10.1016/j.cell.2025.04.008

Continued

REAGENT or RESOURCE	SOURCE	IDENTIFIER
Zebrafish *Tg(bactin2:loxP-BFP-stop-loxP-DsRed)* ^{sd27}	Kobayashi et al.[49]	D. Traver Lab
Oligonucleotides		
Primers	This paper	Table S1
sgRNAs	This paper	Table S1
Deposited data		
The raw sequence data of zebrafish brain cells at three developmental stages	This paper	GSA: CRA023422
Software and algorithms		
GraphPad Prism 9	GraphPad Software Inc.	https://www.graphpad.com/
ImageJ (version: 1.8.0)	National Institutes of Health	https://imagej.nih.gov/ij/

EXPERIMENTAL MODEL AND STUDY PARTICIPANT DETAILS

Zebrafish husbandry

Adult Zebrafish (*Danio rerio*) were kept in a circulating system at 28°C under a 14h/10h light/dark cycle. All animal protocols were reviewed and approved by the Animal Care and Use Committee of the Center for Excellence in Brain Science and Intelligence Technology, Chinese Academy of Sciences (NA-046-2023). Transgenic zebrafish larvae are in *nacre* background.[80] Larvae were fed with brachionid rotifers from 4.5 to 9 dpf, and then transition to being fed with Artemia thereafter. The 9-dpf larvae used for experiments in this study measured approximately 5 - 6 mm in length, while the 16-dpf larvae measured approximately 8 - 10 mm in length. The body length of a larva was measured from the snout to the tip of the tail. The sex of embryonic and larval zebrafish was not determined.

Zebrafish lines

The *lyve1b* promoter,[31] *kdrl* promoter,[81] and *uas* promoter[77] were used to label zebrafish muLECs, ECs, neurons, and *Gal4+* cells, separately. The following lines were used: *Tg(lyve1b:DsRed)*, *Tg(lyve1b:DsRed-P2A-nGFP)*, *Tg(kdrl:EGFP)*^{s843},[79] *Tg(elavl3:GCaMP6s)*^{a13203},[73] *Tg(elavl3:NES-jRGECO1a)*^{ion72dTG},[74] *Tg(gfap:NTR-mCherry)*, *Tg(2×en.cpce:tdTomato-CAAX)*,[76] *Tg(elavl3:ChrimsonR-tdTomato)*^{ion57dTg},[75] *Tg(uas:GCaMP6s)*,[78] *Tg(uas:mNeonGreen-P2A-vegfc)*, *Tg(uas:mNeonGreen-P2A-mvegfc)*, *Tg(uas:NTR2.0-P2A-EGFP)*, *Tg(uas:mNeonGreen-P2A-sflt4)*, *Tg(uas:mNeonGreen-P2A-Cre)*, *Tg(bactin2:loxP-BFP-stop-loxP-DsRed)*^{sd27},[49] *Tg(uas:CoChR-EGFP-P2A-H2B-mScarlet)*, *Ki(vegfc-GFF)*, *Ki(vegfd-GFF)*, *Ki(slc6a11b-GFF)*, *Ki(pdgfra-GFF)*, *Ki(pdgfra-DsRed)*, *Ki(ccbe1-GFF)*, *vegfc*^{fl}, *vegfc*$^{-/-}$, and *vegfd*$^{-/-}$ lines.

METHOD DETAILS

Generation of transgenic zebrafish lines

The cDNAs of nitroreductase 2.0 (NTR 2.0),[46] soluble *VEGFR3* (*sflt4*),[30] zebrafish *vegfc* (full coding sequence of 1188 bp for 396 animo acids), zebrafish mature *vegfc* (*mvegfc*, coding sequence of 1 - 57 bp for signal peptide, and 274 - 642 bp for VEGF homology domain) and Cre were cloned into a *uas:mNeonGreen* or a *uas:EGFP* vector to construct the *uas:mNeonGreen-P2A-vegfc*, *uas:mNeonGreen-P2A-mvegfc*, *uas:NTR2.0-P2A-EGFP*, *uas:EGFP-P2A-sflt4* and *uas:mNeonGreen-P2A-Cre*. *CoChR-EGFP* and *P2A-H2B-mScarlet* were combined into the *uas:P2A-EGFP* vector to synthesize the plasmid *uas:CoChR-EGFP-P2A-H2B-mScarlet*, enabling labeling both the cell membrane and nucleus. Transgenic lines were generated with the *Tol2* system,[82] by co-injection of the above plasmids (25 ng/μl) and the *Tol2* transposase mRNA (25 ng/μl) into one-cell stage embryos.

CRISPR/Cas9-mediated knockin

Ki(vegfc-GFF), *Ki(vegfd-GFF)*, *Ki(slc6a11b-GFF)*, *Ki(pdgfra-GFF)*, *Ki(pdgfra-DsRed)* and *Ki(ccbe1-GFF)* knockin lines were generated with the method we established previously,[41,42] which preserves the integrity of the targeted endogenous gene. Briefly, sgRNAs targeting the last intron of each gene were selected with CRISPOR online serve (http://crispor.tefor.net/crispor.py). The sgRNAs with 2′-O-methyl-3′-phosphorothioate modification at both ends were synthesized by GenScript. For making knockin donor plasmids, the left arm and right arm of each gene were amplified by PCR with the indicated primers in Table S1 and cloned into a *P2A-GFF* backbone vector. Each one-cell-stage embryo was injected with 1-nl RNAase free liquid mixture, containing 600 pg SpCas9 protein, 125 pg sgRNA and 25 pg donor plasmid. To screen the founder of each knockin line, the adult F0 was crossed with WT fish, and the genome DNA of the F1 embryos was extracted at 4.0 dpf, and was used to PCR using the primers shown in Table S1.

Please cite this article in press as: Li et al., Neural-activity-regulated and glia-mediated control of brain lymphatic development, Cell (2025), https://doi.org/10.1016/j.cell.2025.04.008

CRISPR/Cas9-mediated knockout

The knockout lines of *vegfc*$^{-/-}$ and *vegfd*$^{-/-}$ were generated with the CRISPR/Cas9 system. We selected the appropriate sgRNAs (Table S1) targeting the sequence of the exon 6 of *vegfc* and the exon 2 of *vegfd*, respectively. 1 nl RNAase free liquid mixture containing 500 ng/μl SpCas9 protein and 125 ng/μl sgRNA was injected at the single-cell stage. Genotyping of *vegfc*$^{-/-}$ and *vegfd*$^{-/-}$ knockout fish was performed using primers in Table S1. The *ccbe1* crispants were generated by injection of 1 nl RNAase free liquid mix of two sgRNAs (125 ng/μl each) targeting the exon 1 and exon 2 of *ccbe1* with SpCas9 protein (500 ng/μl) as previously reported.[83]

Generation of a *vegfc*^{fl} allele

High-efficiency sgRNA target sites were selected (Table S1) in the intron 3 of the *vegfc* gene, and then a 100-bp sequence upstream of the sgRNA site was used to combine with the inverted cassette with the *loxP* site, splice acceptor, TagRFP, BGHpA, and GAPDH *3′UTR*, along with the exon 4, exon 5, exon 6, and exon 7 of *vegfc* as the left arm of the donor plasmid *vegfc*^{fl}. The right arm of this donor was the same as the knockin donor plasmid *vegfc-GFF*. To facilitate the identification of offspring carrying the *vegfc*^{fl} allele, we inserted *myl7-EGFP* in front of the left arm to simultaneously label the heart in green, and finally obtain the *vegfc*^{fl} donor plasmid. Ultimately, SpCas9 protein, sgRNA, and *vegfc*^{fl} donor plasmid were co-injected into single-cell-stage fertilized eggs. Each embryo was injected with 1 nl solution containing 600 ng/μl SpCas9 protein, 125 ng/μl sgRNA, and 20 ng/μl donor plasmid. To screen for *vegfc*^{fl} founders, we crossed adult fish with nacre wild-type and extracted genomic DNA at 3 dpf. We used PCR (with primers in Table S1) and imaging of green hearts to validate germline transmission.

scRNA-seq library preparation and analysis

Fresh zebrafish brains administered with papain digestive solution (containing 28 units/ml papain (Gibco) and 0.02 mg/ml DNase (Gibco)) and 0.48 mg/ml L-cysteine) were dissociated at 37°C for 15 min, during which time they were blown intermittently with a pipette for full cracking. The samples were then filtered with a 40-μm cell filter, centrifuged at 800 g for 5 min, and the supernatant was discarded. The cells were re-suspended with PBS containing 0.04% BSA (MACS). Next, the single-cell suspensions were loaded onto a Chromium Single Cell Controller Instrument (10× Genomics) to generate single-cell gel beads in emulsions (GEMs). Following the manufacturer's instructions, reverse transcription, cDNA PCR amplification, and library preparation were conducted. All libraries were sequenced using the Illumina NovaSeq 6000 with 2× 150 bp paired-end reads. Raw sequencing data were processed using Cell Ranger software (10X Genomics, v.5.0.0) to de-multiplex cellular barcodes, map reads to the reference genome, and generate a gene count matrix. The R package Seurat (v.3.1.1) was used for quality control, pre-processing, normalization, clustering, and differential expression analysis. Low-quality cells and likely multiplet captures were removed based on the following criteria: gene numbers less than 200, unique molecular identifier (UMI) counts less than 1000, or $\log_{10}$GenesPerUMI less than 0.7. Additionally, cells with hemoglobin genes ratio greater than 5% or mitochondrial genes ratio greater than 10% were excluded. The DoubletFinder package (v.2.0.2) was used to identify potential doublets.

Multiplexed Fluorescence In Situ Hybridization (FISH) using a customized Hybridization Chain Reaction (HCR) protocol

Zebrafish larvae were first fixed in 4% paraformaldehyde (PFA) for 12 hours and subsequently stored in PBST. Following initial fixation, the larvae underwent post-fixation in 4% PFA for 15 min, followed by sequential dehydration in 50% and 70% ethanol overnight. The samples were then treated twice with 100% ethanol and washed with PBS. To enhance probe accessibility, the larvae were treated with proteinase K (10 μg/mL) at 37°C for 10 min and washed twice with PBS. For hybridization, the larvae were pre-incubated in hybridization buffer at 37°C for 10 min, followed by overnight incubation (>24 hours) at 37°C in a probe solution containing hybridization buffer and custom-designed probes ([*slc6a11b*]: 113024119; [*vegfc*]: 113024122; [*slc1a2b*]: 113024117, synthesized by Sangon Biotech). Excess probes were removed by washing with probe wash buffer at 37°C and 5× SSCT at room temperature. For signal amplification, the samples were pre-incubated in amplification buffer and then incubated overnight at room temperature in the dark with snap-cooled fluorescent hairpins (Molecular Instruments, including two sets of hairpins custom-conjugated with JF669 to minimize photobleaching). After amplification, excess hairpins were removed by washing with 5× SSCT. The processed samples were stored at 4°C in the dark until imaging.

Transient injection for mosaic labeling of the glia

To perform single-cell mosaic analysis, the *uas:CoChR-EGFP-P2A-H2B-mScarlet* construct or *uas:CoChR-EGFP* (5 ng/μl) was injected into fertilized eggs of stable lines of *Ki(slc6a11b-GFF) or Ki(vegfc-GFF)*. The injected embryos were kept at 28.5°C and imaged at 6 dpf or 7 dpf.

Chemical treatment

MTZ treatment was performed as previously described.[46] Zebrafish larvae were treated with 2 mM MTZ dissolved in system water at indicated developmental stages. Then the larvae were washed with system water for three times before imaging. To block neural activity, zebrafish larvae were bathed in system water containing 400 μM tricaine. The pH of the tricaine solution was adjusted to

Please cite this article in press as: Li et al., Neural-activity-regulated and glia-mediated control of brain lymphatic development, Cell (2025), https://doi.org/10.1016/j.cell.2025.04.008

7.2 - 7.5. The tricaine solution was replaced every 12 hours, and larvae were raised until imaging as previously reported.[34,35] The chemically treated larvae with similar brain size and body length as the untreated control larvae were used for experiments.

In vivo confocal imaging of cell morphology and Ca^{2+} activity

Olympus Fluoview 1000 and 3000 confocal microscopes (Olympus) were used for in vivo imaging of muLECs, fibroblasts and RAs with 20× water-immersion objective lens. The live larvae were fixed in 1.2% low- melting point agarose (Invitrogen). The z-stack was set as 2 - 5 μm per slice. The resolution of all the images was either 1024 × 1024 pixels or 800 × 800 pixels. The imaging data were analyzed with ImageJ.

For in vivo confocal Ca^{2+} imaging, GCaMP6s or jRGECO1a was employed as the calcium indicator to monitor Ca^{2+} activities. Zebrafish larvae at 4 dpf, 7 dpf, and 9 dpf were immobilized in 1.5% low-melting agarose. Imaging was carried out at room temperature, using a 20× water-immersion objective on an Olympus Fluoview 3000 confocal microscope. Single or dual-channel Ca^{2+} imaging was performed at a volume rate of 0.5 - 1 Hz in resonant scanning mode. The z-stack was set as 5 μm per slice.

Analysis of Ca^{2+} activity

Ca^{2+} activity images were first aligned along x-y plane by the Rigid Body Method in ImageJ. Individual regions of interest (ROIs) were manually drawn on the OT neuropil area. Fluorescence was calculated as $\Delta F/F_0$ (fluorescence change (ΔF) relative to its basal level (F_0)), with a spontaneous Ca^{2+} activity identified as an event when its peak was larger than 1.5 standard deviation (SD) of the baseline by using a self-written MATLAB program. The area under the curve (AUC) of Ca^{2+} activity events was employed to indicate the strength of neural and glial Ca^{2+} activities. The AUC was calculated using a custom MATLAB program. For glial Ca^{2+} activities induced by optogenetic activation of OT neurons, the averaged peak amplitude of the responses evoked by repetitive stimulations was measured for each experiment.

Visual stimulation by moving bars and flashes

Under full dark, a video projector (MP-CD1, SONY) was used to project a stripe pattern (stripe width: 5 mm) over the side of the dish where the freely moving larvae were placed. The pattern was fixed to move forward at a drift speed of 1 cm/s. 2-dpf larvae were exposed to 14 h of moving bar stimulation and 10 h of full dark. The larvae in the control group were placed under full dark with the same temperature and humidity. To evoke activities in both glia and neurons, flash stimuli were generated by a violet 5-w LED controlled by Master-8 pulse stimulator (A.M.P.I., Israel), and the LED was 5 cm straight ahead from the recording chamber. The light intensity was 550 lux, and the duration was 2 s with a 90-s interval.

Electrical stimulation

The *Tg(lyve1b:DsRed)* larvae at 2 - 6 dpf were used for the electrical stimulation experiment. Larvae were placed in a 4.5 cm × 5.5 cm tank. Parallel silver foil sheets were attached to both long sides of the tank at a voltage of 2.5 V/cm, with wires connected to each sheet. Each stimulation consisted of 5 electrical pulses with a duration of 100 ms and an interval of 5 min. Stimulations were administered twice a day at 8 AM and 6 PM, respectively. The larvae were not fed during the experiment.

Optogenetic activation

Simultaneous optogenetic stimulation of OT neurons and Ca^{2+} imaging of glia were performed using an Olympus Fluoview 3000 confocal microscope. The *Ki(slc6a11b-GFF);Tg(uas:GCaMP6s);Tg(elavl3:ChrimsonR-tdTomato)* larvae were used. Optogenetic stimulation was delivered by 488 nm laser scanning. The excitation intensity was 0.17 mW/mm^2 and the stimulation duration was 1 s with 10-ms pulses at 10 Hz. To avoid visual stimulation introduced by the laser used for optogenetic activation, we performed bilateral eye removal before the experiment.

QUANTIFICATION AND STATISTICAL ANALYSIS

Statistics

Animals were randomly assigned to experimental groups using simple randomization and raised under identical conditions. The normality assumption of the data was tested first. For two-group comparison, the two-tailed paired or unpaired *t*-test was used for significance analysis for normal data. For non-normally distributed data, two-tailed Mann Whiteney *U*-test was used. For multiple-group comparisons, one-tailed one-way ANOVA (Tukey's post-hoc test) was used for normally distributed data, and one-tailed Kruskal-Wallis tests (with post hoc Dunn's test) for non-normally distributed data. Sample sizes, error bars, and exact *p* values are provided in figures and legends. Analysis was performed using GraphPad Prism v9.0 software. Error bar represents SD.

Software

All software is freely or commercially available and is listed in the STAR Methods description and key resources table.

Supplemental figures

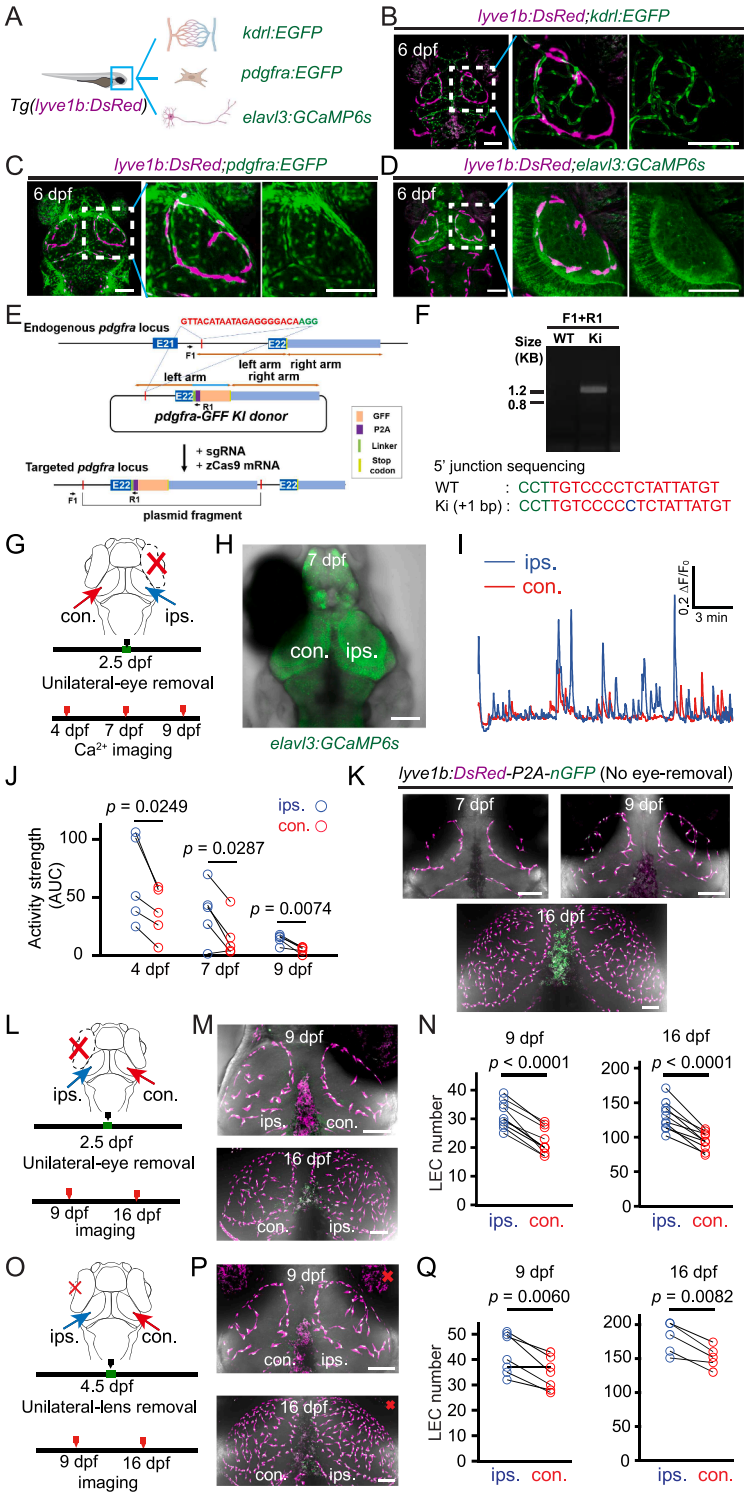

(legend on next page)

Figure S1. Spatial relationship between muLECs and other types of brain cells and the regulation of muLEC development by neural activity, related to Figure 1

(A) A cartoon depicting the co-labeling of muLECs with blood vessels (*Tg(kdrl:EGFP)*, abbreviated as *kdrl:EGFP*); fibroblasts (*Ki(pdgfra-GFF);Tg(uas:EGFP)*, abbreviated as *pdgfra:EGFP*); and neurons (*Tg(elavl3:GCaMP6s)*, abbreviated as *elavl3:GCaMP6s*) in zebrafish, illustrating the spatial relationship between muLECs and these cell types.

(B–D) Dorsal view of projected images of muLECs with blood vessels (B), fibroblasts (C), and neurons (D) at 6 dpf. Left: dorsal view of a projected image of bilateral OT. Right: enlarged view of the area indicated by the dashed boxes in the right image.

(E) Schematic of the design for generating *GFF* knockin at the zebrafish *pdgfra* locus (*Ki(pdgfra-GFF)*) by using an intron-based knockin method via the CRISPR/Cas9 system (see STAR Methods and Choi et al.[43]).

(F) PCR and sequencing of the 5′ junction of *Ki(pdgfra-GFF)* F1 progenies. The F1 and R1 primers are shown in (E). The indel mutation of insertion is shown in blue, and the protospacer adjacent motif (PAM) and sgRNA target sequences are shown in green and red, respectively.

(G–J) Effects of unilateral eye removal on the neural activity in the contralateral OT.

(G) Experimental design for unilateral eye removal and Ca^{2+} imaging of OT neurons. con., contralateral side; ips., ipsilateral side; red cross, eye removal.

(H) Dorsal view of the brain in a 7-dpf *Tg(elavl3:GCaMP6s)* larva with right eye removal.

(I) Spontaneous Ca^{2+} activities of OT neurons in the ipsilateral (blue) and contralateral (red) OT.

(J) Summary of data showing the activity strength (AUC) of spontaneous Ca^{2+} activities of neurons in contralateral and ipsilateral OT. The data were obtained from 5 larvae imaged at three time points.

(K) Representative images of muLECs on bilateral OT in larvae without eye removal. The imaging was performed at 7, 9, and 16 dpf.

(L–N) Effects of unilateral eye removal on muLEC development. Eye removal was performed at 2.5 dpf, and *in vivo* imaging was performed at 9 or 16 dpf.

(L) Experimental design for unilateral eye removal and imaging. con., contralateral side; ips., ipsilateral side; red cross, eye removal.

(M) Representative images of the eye-removed larvae at 9 (up) and 16 dpf (bottom).

(N) Mean number of muLECs on each side of the OT in the larvae with eye removal at 9 (left) and 16 dpf (right). The data were obtained from 10 larvae in three independent experiments for each group.

(O–Q) Effects of unilateral lens removal on muLEC development. Lens removal was performed at 4.5 dpf, and imaging was performed at 9 or 16 dpf.

(O) Experimental design for unilateral lens removal and imaging. con., contralateral side; ips., ipsilateral side; red cross, lens removal.

(P) Representative images of the lens-removed larvae at 9 (up) and 16 dpf (bottom).

(Q) Mean number of muLECs on each side of the OT in the larvae, with lens removal at 9 (left) and 16 dpf (right). The data were obtained from 7 larvae at 9 dpf and 5 larvae at 16 dpf in two independent experiments.

Scale bars: 100 μm in all images. The *p* values were determined using the parametric two-tailed paired t test (J, N, and Q). Data are represented as mean ± SD.

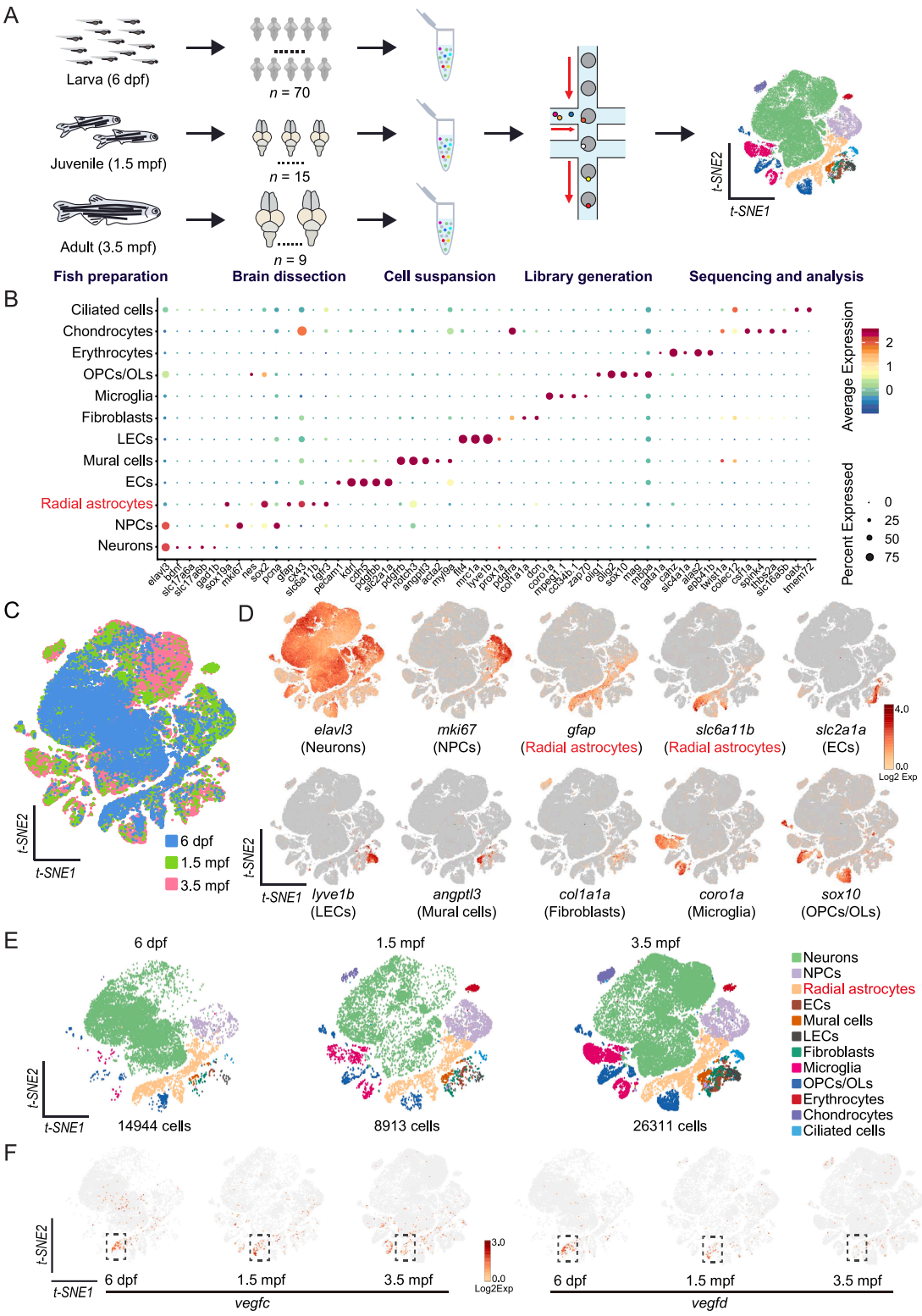

Figure S2. scRNA-seq analysis of whole-brain cells in zebrafish, related to Figure 2

(A) Experimental schematic illustrating the isolation of whole-brain cells from zebrafish at 6 dpf, 1.5 mpf, and 3.5 mpf for scRNA-seq. The numbers indicate the number of animals used.

(legend continued on next page)

(B) Dot plot showing the top marker genes for the twelve cell types of brain cells. The dot size indicates the percentage of cells expressing the genes, and the dot color indicates the average expression level in the cells.
(C) *t*-SNE merged projection of all the whole-brain cells at 6 dpf, 1.5 mpf, and 3.5 mpf.
(D) *t*-SNE expression of ten marker genes. The color bar represents gene expression level.
(E) *t*-SNE projections of the whole-brain cells at 6 dpf, 1.5 mpf, and 3.5 mpf.
(F) *t*-SNE expression of *vegfc* (left) and *vegfd* (right) in the whole-brain cells at 6 dpf, 1.5 mpf, and 3.5 mpf. The color bar represents gene expression level.

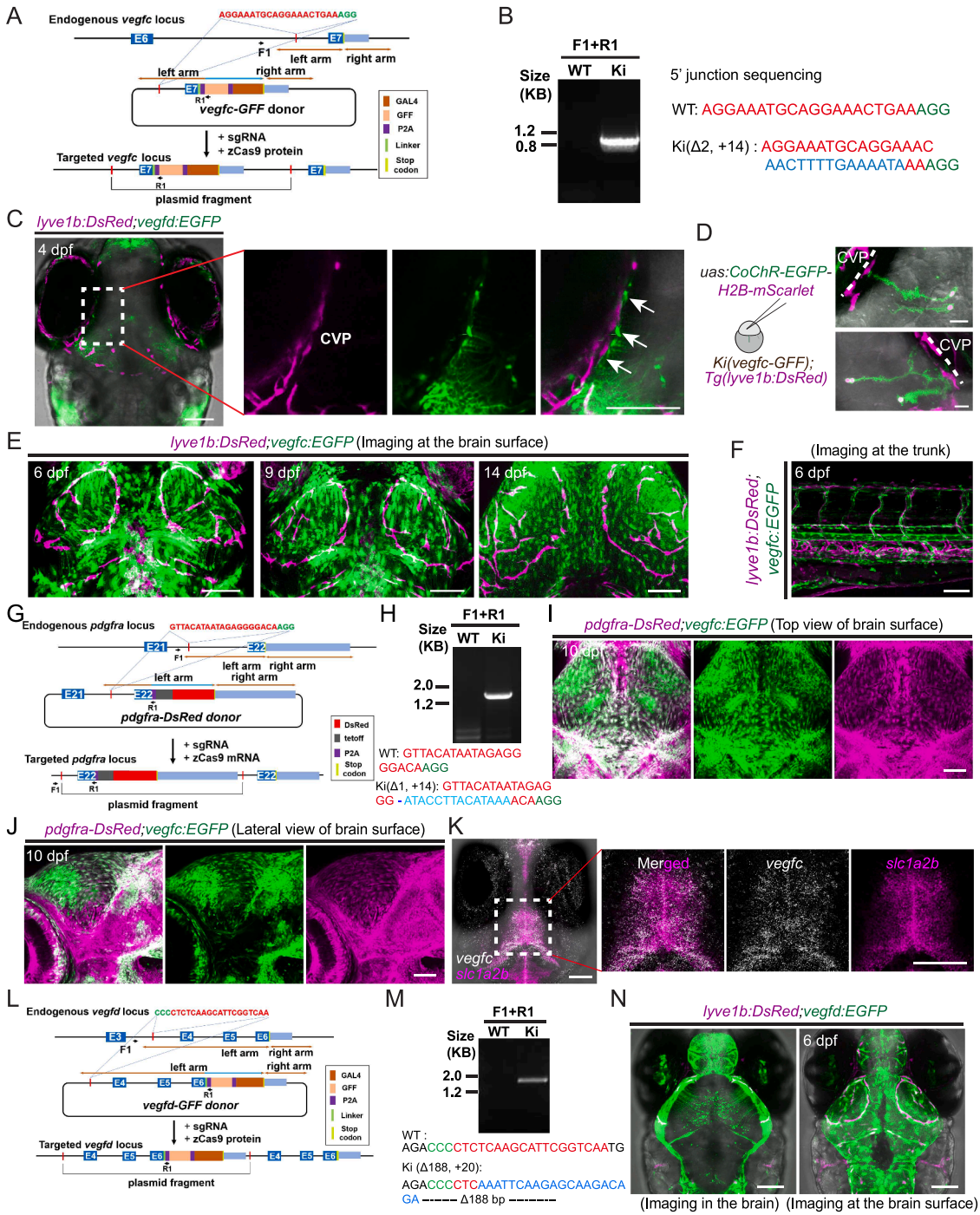

Figure S3. Generation of *Ki(vegfc-GFF)*, *Ki(vegfd-GFF)*, and *Ki(pdgfra-DsRed)* lines for specific labeling of *vegfc*+ RAs, *vegfd*+ Ras, and *pdgfra*+ fibroblasts, related to Figure 2

(A) Schematic of the design for generating *GFF* knockin at the zebrafish *vegfc* locus (*Ki(vegfc-GFF)*) by using an intron-based knockin method via the CRISPR-Cas9 system.

(B) PCR and sequencing of the 5′ junction of *Ki(vegfc-GFF)* F1 progenies. The F1 and R1 primers are shown in (A). The indel mutation of insertion is shown in blue, and the PAM and sgRNA target sequences are shown in green and red, respectively.

(C) Left: dorsal image showing that the endfeet of *vegfc*+ RAs make contact with muLECs at CVP. Imaging was performed on a 4-dpf *Tg(lyve1b:DsRed);Ki(vegfc-GFF);Tg(uas:EGFP)* larva (abbreviated as *lyve1b:DsRed;vegfc:EGFP*). Right: enlarged view from the area indicated by the dashed box in the left image, with white arrows pointing to the contact points between the *vegfc*+ RAs endfeet (green) and muLECs (red).

(legend continued on next page)

(D) Sparse labeling and *in vivo* imaging of individual *vegfc*+ RAs for visualizing their distinct morphology and localization. Left, cartoon depicting the injection of the plasmid *uas:CoChR-EGFP-P2A-H2B-mScarlet* into a fertilized egg of *Ki(vegfc-GFF)* for sparse labeling of individual *vegfc*+ RAs. Right, images showing that the endfeet of *vegfc*+ RAs contact with muLECs at CVP (white dashed lines).
(E) Dorsal view of z stack images at the brain surface of *Tg(lyve1b:DsRed);Ki(vegfc-GFF);Tg(uas:EGFP)* larvae at 6, 9, and 14 dpf, showing *vegfc*+ fibroblasts at the brain surface.
(F) Lateral view of z stacked image at the trunk of *Tg(lyve1b:DsRed);Ki(vegfc-GFF);Tg(uas:EGFP)* larvae at 6 dpf, showing *vegfc* expression in the dorsal aorta, intersegmental arteries, and the horizontal myoseptum.
(G) Schematic of the design for generating *DsRed* knockin at the zebrafish *pdgfra* locus (*Ki(pdgfra-DsRed)*) by using the intron-based knockin method via the CRISPR-Cas9 system.
(H) PCR and sequencing of the 5′ junction of *Ki(pdgfra-DsRed)* F1 progenies. The F1 and R1 primers are shown in (G). The indel mutation of insertion is shown in blue, and the PAM and sgRNA target sequences are shown in green and red, respectively.
(I and J) Dorsal view (I) and lateral view (J) of z stacked images at the brain surface of a 10-dpf *Ki(pdgfra-DsRed);Ki(vegfc-GFF);Tg(uas:EGFP)* larvae (abbreviated as *pdgfra-DsRed;vegfc:EGFP*) larva, showing the co-localization of dsRed and EGFP signals on the brain surface that indicates the expression of *vegfc* in *pdgfra*+ fibroblasts.
(K) z stacked image showing the co-localization of *vegfc* and *slc1a2b* mRNAs. Multiplexed FISH was performed on a whole-mount 6-dpf WT larva by using a customized HCR method with designed probes of *vegfc* (Alexa 647 nm, white) and *slc1a2b* (Alexa 488 nm, magenta).
(L) Schematic of the design for generating *GFF* knockin at the zebrafish *vegfd* locus (*Ki(vegfd-GFF)*) by using an intron-based knockin method via the CRISPR-Cas9 system.
(M) PCR and sequencing of the 5′ junction of *Ki(vegfd-GFF)* F1 progenies. The F1 and R1 primers are shown in (A). The indel mutation of insertion is shown in blue, and the PAM and sgRNA target sequences are shown in green and red, respectively.
(N) Dorsal view of *vegfd*+ RAs inside of the brain (left), and *vegfd*+ fibroblast-like cells on the brain surface (right). The images were taken from a 6-dpf *Tg(lyve1b:DsRed);Ki(vegfd-GFF);Tg(uas:EGFP)* (abbreviated as *lyve1b:DsRed;vegfd:EGFP*) larva.
Scale bars: 20 μm (D) and 100 μm (C, E, F, I–K, and N).

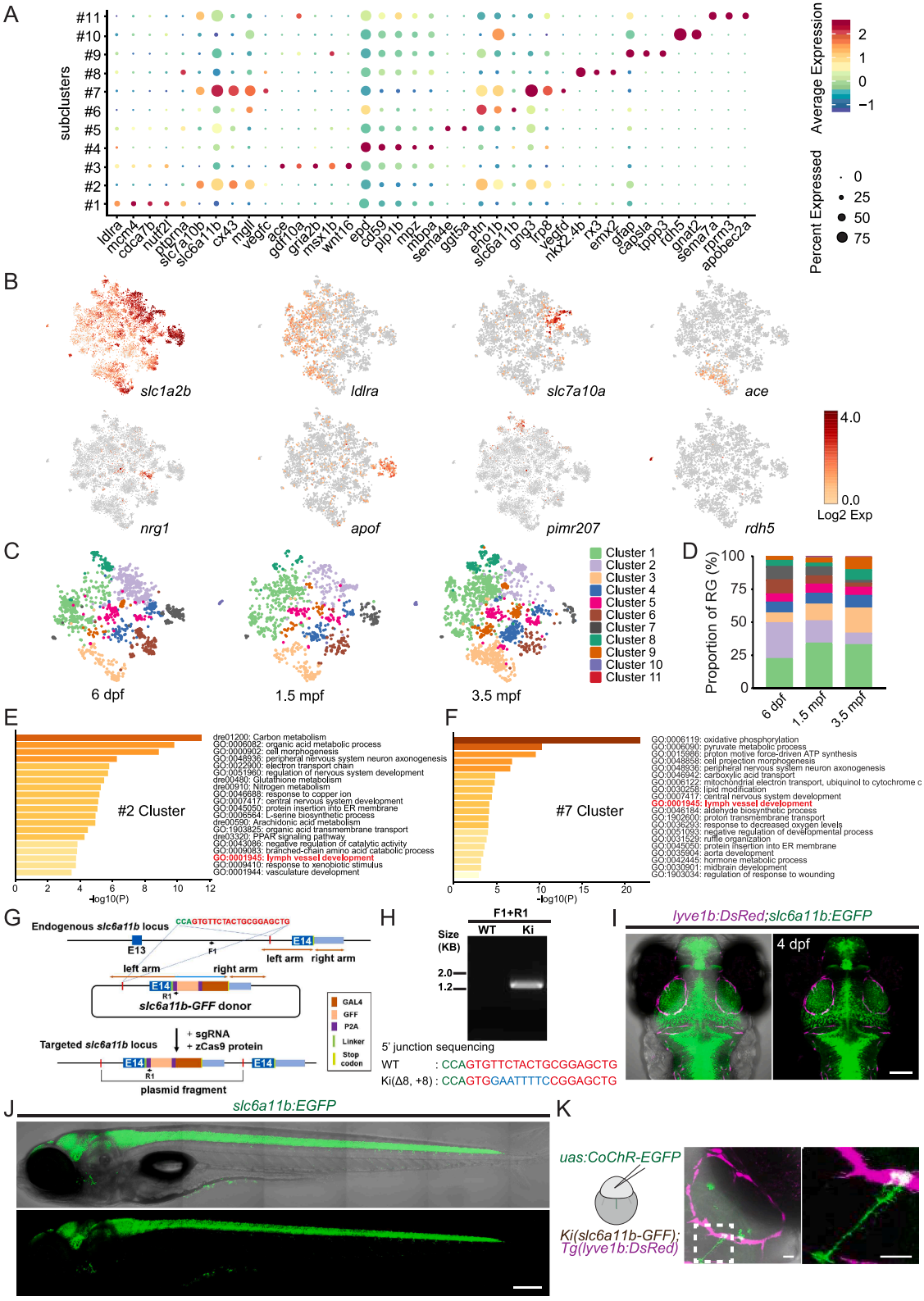

(legend on next page)

Figure S4. scRNA-seq analysis of RA subclusters and generation of the *Ki(slc6a11b-GFF)* line for specific labeling of *slc6a11b+* RAs, related to Figure 2

(A) Dot plot showing the expression of marker genes in the eleven subclusters of RAs. The dot size indicates the percentage of cells expressing the genes and the dot color indicates the average expression level in the cells.

(B) *t*-SNE expression of eight marker genes in the RAs. The color bar represents gene expression level.

(C) *t*-SNE projections showing the eleven subclusters of RAs at 6 dpf, 1.5 mpf, and 3.5 mpf, respectively.

(D) Proportions of the eleven subclusters at 6 dpf, 1.5 mpf, and 3.5 mpf.

(E and F) Metascape analysis of the enriched pathways of #2 (E) and #7 (F) subclusters. The term of lymphatic vessel development is highlighted in red.

(G) Schematic of the design for generating *GFF* knockin at the zebrafish *slc6a11b* locus (*Ki(slc6a11b-GFF)*) by using an intron-based knockin method via the CRISPR-Cas9 system.

(H) PCR and sequencing of the 5′ junction of *Ki(slc6a11b-GFF)* F1 progenies. The F1 and R1 primers are shown in (B). The indel mutation of insertion is shown in blue, and the PAM and sgRNA target sequences are shown in green and red, respectively.

(I) Dorsal view of z stacked images showing that *slc6a11b+* signals are inside of the brain but not on the brain surface. Images were taken from a 4-dpf *Tg(lyve1b:DsRed);Ki(slc6a11b-GFF);Tg(uas:EGFP)* (abbreviated as *lyve1b:DsRed;slc6a11b:EGFP*) larva.

(J) Lateral view of z stacked images of a 6-dpf larva, showing that *slc6a11b+* signals are in the brain as well as spinal cord.

(K) Sparse labeling and *in vivo* imaging of individual *slc6a11b+* RAs for visualizing their distinct morphology and localization. Left: cartoon depicting the injection of the plasmid *uas:CoChR-EGFP* into a fertilized egg of *Ki(slc6a11b-GFF);Tg(lyve1b:DsRed)* for sparse labeling of individual *slc6a11b+* RAs. Right: images showing a *slc6a11b+* RA in contact with the muLEC loop.

Scale bars: 20 μm (K), 100 μm (I), and 200 μm (J).

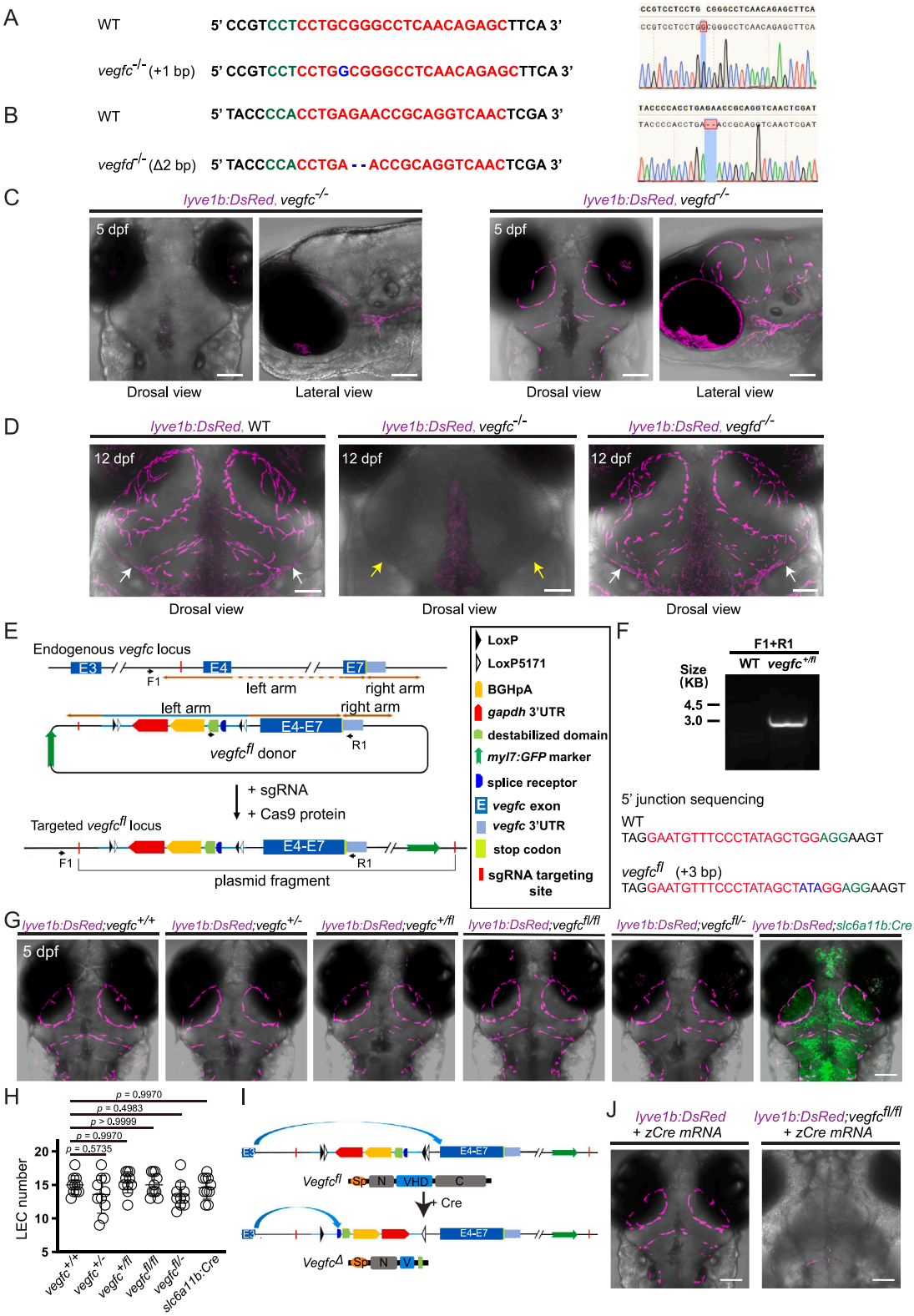

(legend on next page)

Figure S5. Loss of muLECs in *vegfc* but not *vegfd* knockout larvae and the generation of conditional knockout of *vegfc* in *slc6a11b+* RAs, related to Figure 3

(A and B) Schematic and sequencing of *vegfc*$^{-/-}$ (A) and *vegfd*$^{-/-}$ (B). The indel mutation of insertion is shown in blue, and the PAM and sgRNA target sequences are shown in green and red, respectively.

(C and D) Images of muLECs in *vegfc*$^{-/-}$ and *vegfd*$^{-/-}$ at 5 dpf (C, dorsal and lateral views) and at 12 dpf (D, dorsal view). The white arrows indicate intracranial lymphatic vessels on each side of the brain in WT and *vegfd*$^{-/-}$ larvae, and the yellow arrows indicate the loss of intracranial lymphatic vessels in *vegfc*$^{-/-}$ larvae.

(E) Schematic of the design for generating *vegfc*^{fl}.

(F) PCR and sequencing of the 5′ junctions of *vegfc*^{fl} F1 progenies. The F1 and R1 primers are shown in (E). The indel mutation of insertion is shown in blue, and the PAM and sgRNA target sequences are shown in green and red, respectively.

(G and H) Dorsal representative images (G) and the mean numbers (H) of muLECs on each side of OT in 5-dpf *vegfc*$^{+/+}$, *vegfc*$^{+/-}$, *vegfc*$^{+/fl}$, *vegfc*$^{fl/fl}$, *vegfc*$^{fl/-}$, and *Ki (slc6a11b-GFF);Tg(uas:mNeonGreen-P2A-Cre)* (abbreviated as *slc6a11b:Cre*) larvae with the background of *Tg(lyve1b:DsRed)*.

(I) Schematic of the Cre-induced loss of *vegfc* function, achieved by Cre-induced inversion of the *vegfc*^{fl} allele.

(J) Dorsal view of muLECs on bilateral OT from a 5-dpf larva with zebrafish codon-optimized *Cre* (*zCre*) mRNA injection into fertilized eggs of WT (left) and *vegfc*$^{fl/fl}$ (right), with the background of *Tg(lyve1b:DsRed)*.

Scale bars: 100 μm in all images. Error bars represent SD. The *p* values were determined using the parametric one-tailed one-way ANOVA with Tukey's post hoc test.

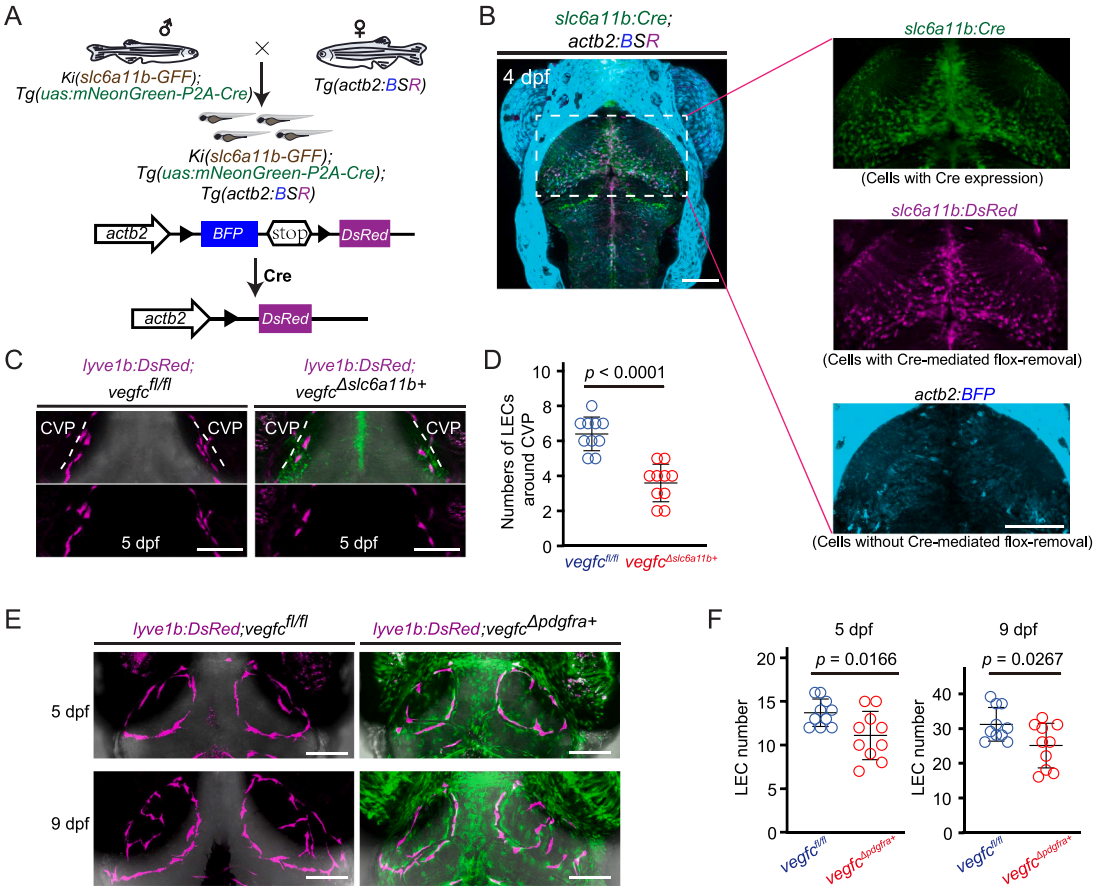

Figure S6. Conditional knockout of *vegfc* in *slc6a11b+* RAs and in *pdgfra+* fibroblasts, related to Figure 3

(A) Schematic for verifying Cre efficiency in *slc6a11b+* RAs. Cre recombinase expression in *slc6a11b+* RAs of *Tg(slc6a11b-GFF);Tg(uas:mNeonGreen-P2A-Cre)* (abbreviated as *slc6a11b:Cre*) specifically excises the floxed DNA cassette between the two LoxP sites in RAs of *Tg(actb2:loxP-BFP-polyA-loxp-DsRed)* (abbreviated as *Tg(actb2:BSR)*), resulting in dsRed expression in *slc6a11b+* RAs and BFP expression in all other types of cells.

(B) Dorsal image of the brain from a *Tg(slc6a11b-GFF);Tg(uas:mNeonGreen-P2A-Cre):Tg(actb2:BSR)* (abbreviated as *slc6a11b:Cre;actb2:BSR*) larva at 5 dpf. The right three images are enlarged view of the area indicated by the dashed box in the left image. mNeonGreen expression indicates the Cre expression in *slc6a11b+* RAs (*slc6a11b:Cre*). dsRed expression in *slc6a11b+* RAs (*slc6a11b:DsRed*) confirms the successful Cre-mediated removal of the floxed DNA cassette between the two LoxP sites in *actb2:BSR*. BFP (expression *actb2:BFP*) marks all other types of cells.

(C and D) Representative images (C) and the mean number (D) of muLECs around the CVP at 5-dpf *vegfc*$^{fl/fl}$ and *vegfc*$^{\Delta slc6a11b+}$ larvae. White dashed lines indicate the CVP. The green signal (C, upper right) indicates the Cre expression in *slc6a11b+* RAs.

(E and F) Representative images (E) and the mean number (F) of muLECs on each side of OT at 5- and 9-dpf *vegfc*$^{fl/fl}$ and *vegfc*$^{\Delta slc6a11b+}$ larvae. The green signal (E, right) indicates the Cre expression in *pdgfra+* fibroblasts.

Scale bars: 100 μm in all images. Error bars represent SD. The *p* values were determined using the parametric two-tailed unpaired t test (D and F). Data are represented as mean ± SD.

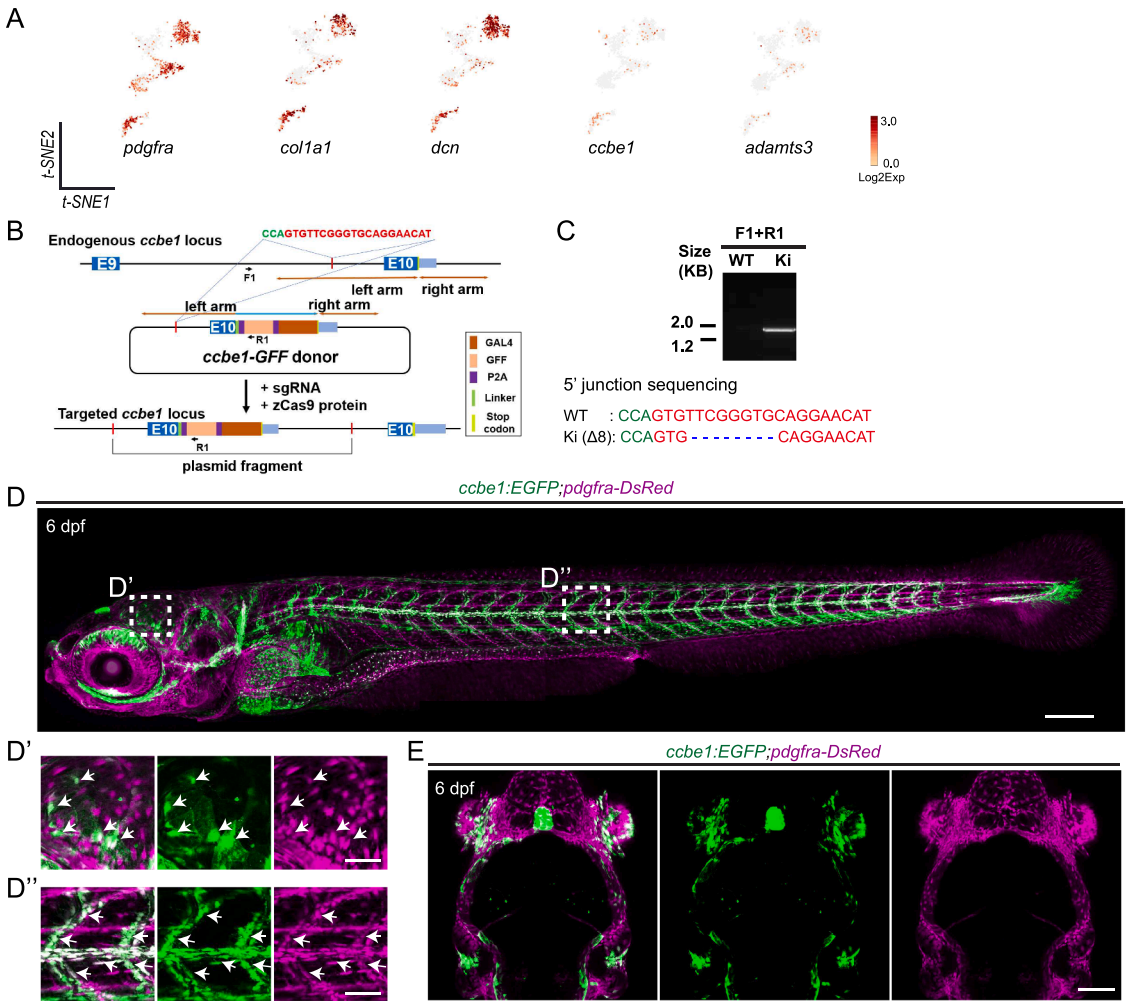

Figure S7. Generation of *Ki(ccbe1-GFF)* for specific labeling of *ccbe1+* cells, related to Figure 6

(A) *t*-SNE expression profiles of the genes in fibroblasts. *pdgfra*, *col1a1*, and *dcn* are marker genes for fibroblasts, and *ccbe1* and *adamts3* are genes encoding proteins that work together to cleave pro-Vegfc into its active mature form.

(B) Schematic of the design for generating *GFF* knockin at the zebrafish *ccbe1* locus (*Ki(ccbe1-GFF)*) by using an intron-based knockin method via the CRISPR-Cas9 system.

(C) PCR and sequencing of the 5′ junction of *Ki(ccbe1-GFF)* F1 progenies. The F1 and R1 primers are shown in (B). The PAM and sgRNA target sequences are shown in green and red, respectively.

(D) Lateral view of a *Ki(ccbe1-GFF);Tg(uas:EGFP);Ki(pdgfra-DsRed)* (abbreviated as *ccbe1:EGFP;pdgfra-DsRed*) larva at 6 dpf.

(D′ and D″) Enlarged images from the two dashed boxes in (D), showing the co-localization (indicated by the white arrows) of *ccbe1+* cells and *pdgfra+* fibroblasts on the brain surface (D′) and in the trunk (D″).

(E) Dorsal view of the inside of the brain from a 6-dpf *ccbe1:EGFP;pdgfra-DsRed* larva.

Scale bars: 50 μm (D′ and D″), 100 μm (E), and 200 μm (D).